

Astrobiology, research article

Cite this article as:

Klenner, F., Postberg, F., Hillier, J., Khawaja, N., Cable, M.L., Abel, B., Kempf, S., Glein, C.R., Lunine, J.I., Hodyss, R., Reviol, R., and Stolz, F. (2020) Discriminating Abiotic and Biotic Fingerprints of Amino Acids and Fatty Acids in Ice Grains Relevant to Ocean Worlds. *Astrobiology* **20**:in press.

---

## **Discriminating Abiotic and Biotic Fingerprints of Amino Acids and Fatty Acids in Ice Grains Relevant to Ocean Worlds**

**Fabian Klenner<sup>1,2#</sup>, Frank Postberg<sup>1,2#</sup>, Jon Hillier<sup>1</sup>, Nozair Khawaja<sup>1,2</sup>,  
Morgan L. Cable<sup>3</sup>, Bernd Abel<sup>4,5</sup>, Sascha Kempf<sup>6</sup>, Christopher R. Glein<sup>7</sup>,  
Jonathan I. Lunine<sup>3,8</sup>, Robert Hodyss<sup>3</sup>, René Reviol<sup>1,2</sup>, and Ferdinand Stolz<sup>4,5</sup>**

<sup>1</sup>Institute of Geological Sciences, Freie Universität Berlin, Malteserstraße 74-100,  
D-12249 Berlin, Germany

<sup>2</sup>Institute of Earth Sciences, Ruprecht-Karls-Universität Heidelberg, Im  
Neuenheimer Feld 234-236, D-69120 Heidelberg, Germany

<sup>3</sup>NASA Jet Propulsion Laboratory, California Institute of Technology, 4800 Oak  
Grove Dr., Pasadena, CA 91109, USA

<sup>4</sup>Leibniz-Institute of Surface Engineering, Permoserstraße 15, D-04318 Leipzig,  
Germany

<sup>5</sup>Wilhelm-Ostwald-Institute for Physical and Theoretical Chemistry, Universität Leipzig, Linnéstraße 3, D-04103 Leipzig, Germany

<sup>6</sup>Laboratory for Atmospheric and Space Physics, University of Colorado, 1234 Innovation Dr, Boulder, CO 80303-7814, USA

<sup>7</sup>Space Science and Engineering Division, Southwest Research Institute, San Antonio, TX 78228-0510, USA

<sup>8</sup>Department of Astronomy and Carl Sagan Institute, Cornell University, Ithaca, NY 14853, USA

#These authors contributed equally to this work.

Corresponding author e-mail: f.klenner@fu-berlin.de

Submitted: 2019 October 26. Accepted for publication: 2020 May 8.

## **Abstract**

**Identifying and distinguishing between abiotic and biotic signatures of organic molecules such as amino acids and fatty acids is key to the search for life on extraterrestrial ocean worlds. Impact ionization mass spectrometers can**

potentially achieve this by sampling water ice grains formed from ocean water and ejected by moons such as Enceladus and Europa, thereby exploring the habitability of their subsurface oceans in spacecraft flybys. Here, we extend previous high sensitivity laser-based analogue experiments of biomolecules in pure water to investigate the mass spectra of amino acids and fatty acids at simulated abiotic and biotic relative abundances. To account for the complex background matrix expected to emerge from a salty Enceladean ocean that has been in extensive chemical exchange with a carbonaceous rocky core, other organic and inorganic constituents are added to the biosignature mixtures. We find that both amino acids and fatty acids produce sodiated molecular peaks in salty solutions. Under the soft ionization conditions expected for low velocity (2 - 6 km/s) encounters of an orbiting spacecraft with ice grains, the unfragmented molecular spectral signatures of amino acids and fatty acids accurately reflect the original relative abundances of the parent molecules within the source solution, enabling characteristic abiotic and biotic relative abundance patterns to be identified. No critical interferences with other abiotic organic compounds were observed. Detection limits of the investigated biosignatures under Enceladus-like conditions are, salinity dependent (decreasing sensitivity with increasing salinity), at the  $\mu\text{M}$  or  $\text{nM}$  level. The survivability and ionization efficiency of large organic molecules during impact ionization appears to be significantly improved when they are

**protected by a frozen water matrix. We infer from our experimental results that encounter velocities of 4 – 6 km/s are most appropriate for impact ionization mass spectrometers to detect and discriminate between abiotic and biotic signatures.**

**Keywords:** Enceladus, Europa, plume, biomarkers, mass spectrometry, space missions

## **1. Introduction**

The subsurface oceans of the Saturnian and Jovian moons Enceladus and Europa, respectively, harbor conditions that appear to be suitable for life or its emergence (Hand et al., 2006; Glein et al., 2018; McKay et al., 2018). Enceladus maintains a cryovolcanic plume (Goldstein et al., 2018; Postberg et al., 2018b; Spencer et al., 2018) and similar venting phenomena are potentially occurring on Europa (Huybrighs et al., 2020; Roth et al. 2014; Sparks et al., 2016, 2017; Jia et al., 2018; Paganini et al., 2019). Measurements by the Cassini spacecraft indicate that a large fraction of the ice particles ejected into space formed from ocean water within Enceladus (Postberg et al., 2009a, 2011a). Sampling these ice grains therefore provides a method for assessing the chemical and physical properties of the

subsurface ocean as well as the ocean-core interface (Postberg et al. 2008, 2009a, 2018a; Hsu et al., 2015; Sekine et al., 2015, Khawaja et al., 2019, Glein and Waite, 2020).

Mass spectrometers like the Cassini spacecraft's Cosmic Dust Analyzer (CDA; Srama et al., 2004), the SURface Dust Analyzer (SUDA; Kempf et al., 2014) being built for NASA's Europa Clipper mission, or instruments proposed for future missions to Enceladus (Lunine et al., 2015; Reh et al., 2016; Mitri et al., 2018), such as the Enceladus Icy Jet Analyzer (ENIJA, Srama et al., 2015), subsequently renamed the Enceladus Ice Analyzer, ENIA, utilize the principle of impact ionization. In these instruments, ions are generated by hypervelocity ( $\geq 1$  km/s) impacts of nm- or  $\mu\text{m}$ -sized grains onto a metal target, forming an impact plasma from which time of flight (TOF) mass spectra are produced (Hillier et al., 2007; Postberg et al., 2009b, 2011b; Wiederschein et al., 2015; Klenner et al., 2019). The impact ionization process creates singly charged ions almost exclusively, and the spectral peak positions, i.e. ion arrival times, therefore only depend upon the atomic and molecular masses, together with the spectrometer's field configuration.

The controlled acceleration of  $\mu\text{m}$ -sized ice grains to hypervelocities in a laboratory environment for instrument calibration is extremely technically challenging, and techniques employing Laser Induced Liquid Beam Ion Desorption (LILBID; Karas et al., 1990, 1991, 2000) have instead been developed to simulate the process

(Postberg et al., 2009a; Wiederschein et al., 2015; Klenner et al., 2019; Taubner et al., 2020). Using such a LILBID analogue experiment, Klenner et al. (2019) reproduced ice grain mass spectral variations as produced by different ice grain impact speeds recorded by CDA at Saturn. In addition to the ability to reproduce non-compositional spectral variations, a further advantage with the analogue laser-desorption approach is that the compounds tested and their concentrations in the water matrix are known. This allows the compositions of ice grains detected in space to be investigated in detail by comparing them with the laboratory data (Postberg et al., 2009a, 2018a; Khawaja et al., 2019).

Data obtained by Cassini's CDA instrument also revealed that ~25 % (by number) of the ice grains formed from Enceladus' salty ocean contain organic material at detectable concentrations (Postberg et al., 2008, 2011a, 2018b). Volatile organic constituents including aliphatic oxygen- and nitrogen-bearing compounds have been identified in the majority of these organic-bearing ice grains (Khawaja et al., 2019). It was found that 5 – 10 % of the organic-enriched ice grains contain even more complex organics derived from refractory macromolecules at high ( $\geq 0.5$  wt.-%) concentrations (Postberg et al., 2018a).

However, given the insufficient mass resolution of CDA, it is still unclear whether these ice grains contain biosignatures. The volatile organics are suggested to have been previously dissolved in the ocean (Khawaja et al., 2019). Their high vapour

pressures enable efficient evaporation from Enceladus' oceanic water, and they subsequently undergo recondensation and adsorption onto water ice nucleation cores upon cooling during ascent through the icy crustal cracks (Postberg et al., 2018b; Bouquet et al., 2019, Khawaja et al., 2019). In contrast, the refractory and probably hydrophobic macromolecules are hypothesized to originate from an organic layer floating on top of the ocean (Postberg et al., 2018a; Figure 1).

Among potential biosignatures, amino acids and fatty acids are considered to be particularly diagnostic (McKay et al., 2018). Techniques such as laser-induced fluorescence (LIF) have been proposed for detecting such biosignatures at low concentrations (e.g. 0.4 ppm of an amino acid in 3  $\mu\text{g}$  of ice collected over an  $\sim 150$  km path) during plume traversing Enceladus flybys (Mathies et al., 2017). Recently, an experimental setup also applicable to ocean world space missions has demonstrated that amino acids and lauric acid can be identified in pure water by chemical ionization mass spectrometry, although the exact sensitivity of this technique remains to be determined (Waller et al. 2019).

High sensitivities to such compounds in pure water have been achieved with a LILBID setup by Klenner et al. (2020), who investigated the cation and anion spectra of various biogenic amino acids, fatty acids with 12 to 20 carbon atoms, and peptides with up to four amino acid residues in pure water. Molecular peaks and characteristic fragments were found to be clearly identifiable, with detection

limits at the  $\mu\text{M}$  to  $\text{nM}$  level. While most amino acids and peptides could be best identified in cation spectra, anion spectra were more suitable for the characterization of fatty acids. Molecular peaks of amino acids at a given concentration vary by more than an order of magnitude in intensity because of the different  $\text{pK}_a$ -values and proton affinities of individual amino acids. In contrast, molecular peaks of fatty acids at a given concentration are almost equally high (Klenner et al., 2020).

Building on the foundation of Klenner et al. (2020), here we investigate two additional key aspects required for the characterization of these potential biosignatures if embedded in ice grains emerging from a subsurface ocean and ejected by an Enceladus-like plume.

- a) The example of Enceladean ice grains shows that some biosignatures might not be present in relatively pure water ice and instead will coexist with additional inorganic and organic constituents. We investigate the effects of ocean constituents other than water on the spectral appearances and on the detection limits of biosignatures.
- b) Both amino acids and fatty acids are also found in abiotic environments (Cronin and Pizzarello, 1983; Altwegg et al., 2016). However, the abundance ratios of specific amino acids and fatty acids which result from abiotic and biotic generation are distinctly different. We investigate abundances from both

sources with the LILBID experiments to predict characteristic mass spectrometric fingerprints for abiotic and biotic cases in impact ionization mass spectrometers on future space missions.

The abiotic synthesis of amino acids in water-rock systems (e.g. Menez et al., 2018) follows the free energy of formation with the abundance of the simplest amino acid glycine exceeding those of other, more complex amino acids (Higgs and Pudritz, 2009). Because abiotic synthesis is generally inefficient, kinetically controlled reactions should favor the synthesis of simpler amino acids. In contrast, in biotic systems the more complex amino acids become prevalent and therefore the ratio of different amino acids to glycine can be used as a biosignature (Dorn et al., 2011; Davila and McKay, 2014; Reh et al., 2016; Sherwood, 2016; Creamer et al., 2017).

Fatty acids can also aid in the search for life, as they are commonly present in the lipid membranes of Earth life. For most organisms (bacteria and eukaryotes), fatty acids are biochemically produced by the addition of two carbon atoms at a time, resulting in an excess of unbranched, saturated fatty acids with an even number of carbon atoms, with hexadecanoic acid ( $C_{16}$ ) and octadecanoic acid ( $C_{18}$ ) dominating (Georgiou and Deamer, 2014). For archaea, carbon chains are constructed from isoprene units, and hence exhibit a 5-carbon pattern (Berg et al., 2012). In contrast, in the abiotic (e.g., Fischer-Tropsch) synthesis of carbon chains, carbon atoms are added one at a time. The relative abundances of fatty acids with

different backbone lengths can therefore serve as a discriminator for biosignatures (Dorn et al., 2011; Reh et al., 2016; Sherwood, 2016; Summons et al., 2008), although these patterns may be significantly less apparent in psychrophilic organisms that use more branched and unsaturated fatty acids to maintain membrane flexibility (M.J. Malaska, pers. comm., 2019). In addition to mere detection, the ability to differentiate between biotic and abiotic signatures on extraterrestrial ocean worlds might therefore be crucial in the search for life.

The effects of ocean constituents other than water on the spectral appearance and detection limits for the above-mentioned key organic species are of particular relevance to ocean worlds. Sodium salts, believed to be endogenous, have not only been observed on the surface of Europa (Trumbo et al. 2019), but also in particles emitted by Enceladus, where a large fraction of the ice grains detected in the plume are thought to be frozen ocean spray (called Type 3 grains). There, the non-water constituents are dominated by sodium salts amounting to about 1% of the ice grain's mass (Postberg et al. 2009a, 2011a). These salts produce large quantities of cations and anions upon impact ionization and may suppress the signals arising from less abundant dissolved constituents or modify their spectral appearance (Annesley, 2003; Piwowar et al., 2009). Amino acids are quite soluble (Dunn et al., 1933) and, if present, will dissolve in Enceladus' salty ocean and can be expected to reside in the salty Type 3 ice grains. Thus, in this work we investigate amino acids in an

Enceladus-like salty ocean scenario and examine the effects of sodium salts on the mass spectral appearance as well as detection limits of the amino acids.

Although the Enceladean ocean is alkaline (e.g., Postberg et al. 2009a; Glein et al., 2015, 2018) and contains sodium (e.g. Postberg et al., 2009a), it is reasonable to assume that long-chain fatty acids, due to their low solubility in water, are not significantly dissolved in the ocean at temperatures close to 0 °C, but instead are part of a phase-separated organic layer on top of the water surface (as described in Postberg et al. (2018a)). After these components are aerosolized, they could serve as condensation cores for water vapor within the south polar ice vents, thereby growing a salt-poor outer ice layer on the grain (Postberg et al., 2018a,b). We therefore investigate appropriate mixtures of different fatty acids in a salt-poor solution and differentiate between biotic and abiotic signatures in the corresponding mass spectra.

In addition to potential biosignatures and salts, other organic species, most notably low-mass carboxylic acids, which are abundant in carbonaceous chondrites (Huang et al., 2005), could coexist in the ice grains. The latter species could be derived from a primordial reservoir in carbonaceous rock at the bottom of the ocean. We therefore investigate a complex mix of amino acids together with fatty acids and other organic background compounds, to identify potential interferences and infer

how readily biosignatures from these key organic species can be detected in such a complex mixture.

## **2. Methods**

Analogue mass spectra were generated by the LILBID mass spectrometer acting upon water or water-acetonitrile matrixed solutions (see section 2.2). Here the LILBID process, and the variety and concentrations of the solutions used, are described.

### **2.1 Experimental**

The experimental setup used for this work (Figure 2) is described in detail in Klenner et al. (2019) and we therefore provide only a brief overview here.

The technique used to simulate the impact ionization process of ice grains in space is as follows. A  $\mu\text{m}$ -sized liquid water beam is irradiated by a pulsed infrared laser (20 Hz and 7 ns pulse length) operating at a wavelength of approximately 2850 nm and at variable laser intensities (0 – 100 %). The water beam absorbs the laser energy and explosively disperses into atomic, molecular and macroscopic fragments, a portion of which is charged. After passing through a field-free drift region, cations and anions are analyzed in a commercial reflectron time-of-flight mass spectrometer (TOF-MS). The mass spectrometer uses the principle of delayed

extraction (Klenner et al., 2019). The delay time between laser shot and the switch-on of the acceleration voltages of the mass spectrometer, during which ions traverse the field-free region and enter the acceleration region, is adjusted, which allows the extraction of the ions as a function of their initial velocities. After amplifying and digitizing the detected signals, the final mass spectrum is recorded with a LabVIEW-controlled computer. The mass spectra presented here are each an average of typically 500 individual spectra, co-added to improve the signal to noise ratio. The experimental setup is intensity calibrated before every measurement by using a  $10^{-6}$  M NaCl solution at three different delay times and laser intensities to ensure reproducible spectra. The mass spectra typically achieve a mass resolution of 600-800  $m/\Delta m$  (Full Width at Half Maximum, FWHM).

## **2.2. Biosignature solutions**

Three main compositional scenarios have been investigated using four different types of solution (i, ii, iii, and iv below). In the following, amino acids are abbreviated to their common three letter codes (see Table 1) and fatty acids to their respective carbon number  $C_n$ .

### **2.2.1 Amino acids in a salt-rich solution**

#### Solution type i

Initially, 100 ppmw of the single amino acids *His* and *Arg*, each in a separate 0.1 M NaCl solution, were measured to investigate the general spectral appearance of amino acids under salty ocean conditions. Detection limits of each of the following ten amino acids under such conditions were determined: *Asp*, *Glu*, *His*, *Arg*, *Cit*, *Gly*, *Ser*, *Thr*, *Orn*, and *Tyr*. A characteristic mass peak just exceeding a  $3\sigma$  signal to noise level was defined as the detection limit.

#### Solution type ii

These experiments were designed to investigate the mass spectra from ice grains that preserve the composition of a hypothetical abiotic ocean on Enceladus.

The abiotic abundances of amino acids and other soluble organic constituents are calculated under the simplified assumption that Enceladus' rocky core has a composition similar to primitive CR chondrites and that all water-soluble organics are unlikely to remain for long timescales in the highly porous, water-percolated (Choblet et al., 2017) rocky core, instead leaching into the ocean water. Organic abundances in CR2 and CR3 chondrites were reported by Glavin et al. (2011) and Pizzarello et al. (2012). We use the average concentrations (nmol/kg) of the seven most abundant amino acids, and those of the fourteen other most abundant soluble organic compounds (Table S1), dissolving their total mass in the entire ocean volume. Estimates of the mass of the rocky core and the Enceladus ocean were

obtained from Waite et al. (2017). An example calculation and the resulting concentrations of the amino acids and carboxylic acids are summarized in Supplementary Material 1 and Table S1. Concentrations of the most abundant inorganic substances were inferred by using values for the most abundant salts (0.1 M NaCl, 0.015 M Na<sub>2</sub>CO<sub>3</sub>, and 0.015 M NaHCO<sub>3</sub>) from Postberg et al. (2009a) and adopting an NH<sub>3</sub> concentration of 0.01 M (Waite et al., 2017).

## 2.2.2 Fatty acids in a salt-poor solution

### Solution type iii

In contrast to amino acids, long-chain fatty acids are thought unlikely to be present at high concentrations in the salty ocean water because of their low water solubilities. They instead may accumulate in a thin organic film/layer on top of the water surface (Postberg et al., 2018a). Making combined solutions in the laboratory, at concentrations in pure water approaching the upper limit for the nine fatty acids (C<sub>12-20</sub>), was found to be unfeasible and instead an acetonitrile-water mixture (50:50 vol) was used together with the sodium salts (soaps) of the fatty acids (as in Klenner et al., 2020). This enabled the required concentrations to be achieved and also introduced small amounts of sodium into the solution as might be expected in the organic layer on Enceladus (Postberg et al., 2018a) from physical mixing during the disruption of this layer (Figure 1).

Abundances of abiotically produced fatty acids in carbonaceous chondrites range from 100 ppbw to 5 pptw (Hayes, 1967; Lai et al., 2019); leaching from the chondrite-like core of Enceladus (Sekine et al., 2015) would generate dissolved free fatty acids (DFFA) in the ocean in the ~20-200 micromolar range (Waite et al., 2017). Abiotic fatty acid synthesis, via e.g. Fischer-Tropsch-type processes (Loison et al., 2010), results in no preference for the production of odd or even carbon number fatty acids (see Introduction). We therefore consider the solution investigated by Klenner et al. (2020), with each saturated fatty acid at a concentration of  $5.5 \times 10^{-6}$  M, as a possible lower bound. By contrast, many biochemically-produced fatty acids show a clear preference for even carbon number fatty acids over odd carbon number fatty acids, with C<sub>16</sub> and C<sub>18</sub> showing the highest abundances (Georgiou and Deamer, 2014; see Introduction). To investigate the spectral appearance of a simplified biotic vs. an abiotic fatty acid fingerprint at comparable concentrations, a solution with the odd carbon number fatty acids (saturated) at a concentration of  $5.5 \times 10^{-6}$  M, C<sub>12</sub>, C<sub>14</sub> and C<sub>20</sub> at a concentration of  $55 \times 10^{-6}$  M (10-fold greater than the odd-carbon background) and C<sub>16</sub> and C<sub>18</sub> at a concentration of  $275 \times 10^{-6}$  M (50-fold greater) was prepared and analyzed. Concentrations in ppmw can be found in Supplementary Table S2. Due to the use of the sodium salts, this resulted in a [Na]<sup>+</sup> concentration of about 0.75 mmol/L in the solutions used.

### 2.2.3 Complex biosignature mix

#### Solution type iv

We also investigate a more complex case in which amino acids and fatty acids enter the Enceladus ocean from biotic processes at depth. The fatty acids are assumed to migrate upwards through the oceanic layer by thermal convection and bubble transport, thereby accumulating in an organic layer at the ocean's surface (Porco et al. 2017, Postberg et al., 2018a). Droplets formed from this layer may become the cores of salt-poor ice grains (Figure 1) after they are aerosolized from bubble bursting (Postberg et al. 2018a).

We based our concentration estimates on Earth's ocean as an analogue, as amino acid concentrations are determined by life as a system, which produces and consumes them. The presence of specific amino acids (e.g. aspartic acid and arginine) indicates either active biotic or abiotic production because these amino acids are degraded over relatively short geologic timescales ( $< 1$  Ma) (Truong et al., 2019). Ocean concentrations of dissolved free amino acids (DFAAs) are 10-20 nM in the deep ocean (Repeta, 2014), equivalent to about 1 ppbw *Gly*. The average concentration of dissolved free fatty acids (DFFAs) in ocean water is 5-80  $\mu\text{g/L}$  or 5-80 ppbw (Zsolnay, 1977). We adjust this value based on enrichment of organics in marine sea spray aerosols, which was found to be a good analogue for organic enriched ice grains from Enceladus (Postberg et al. 2018a). Russel et al. (2010)

observed that bulk organic compounds are 100 – 1000 times enriched in marine aerosols compared to the surface ocean. From these, lipids and proteins will be even more (preferentially) enriched in sea spray aerosols (Burrows et al. 2014 & references therein). For our biotic solution, we choose to enrich fatty acids by a factor of ~100 and amino acids by a factor of ~1000, yielding values slightly above or below 1 ppmw for each component.

To mimic abundance variations from biogenic fatty acids, we reduced the concentrations of fatty acids with odd carbon numbers and enhanced it 10-fold or 50-fold for fatty acids with even carbon numbers as done previously in Solution type iii. Ratios (varying from 0.25 to 1.5) of biogenic amino acids relative to *Gly* were approximated using values for interstitial ocean water from Kawahata and Ishizuka (1992). To account for other organics that may be likewise embedded in the ice grains (see Introduction), we added the same 14 carboxylic acids as used for Solution type ii, plus propionic acid, each at higher concentrations than the biogenic compounds, to represent abiotic organic background components in a salt-poor solution. The concentrations of all substances used in Solution type iv are summarized in Table S3.

### **3. Results and spectral analysis**

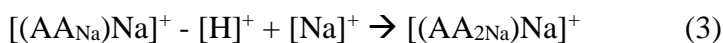
Measurement results for the four types of solutions (i, ii, iii, iv) are presented below. The laboratory results are archived in the form of an internal database (spectral reference library) and can be compared with results from previous and future space missions.

### **3.1 General spectral appearance of amino acids and their detection limits in salty solutions (Solution type i)**

In a typical cation mass spectrum of an amino acid (AA) in a salty solution (Solution type i), the spectral ‘background’ produced by the NaCl solution consists of peaks of the form  $[(\text{H}_2\text{O})_n\text{Na}]^+$ ,  $[(\text{NaOH})_n\text{Na}]^+$ ,  $[(\text{NaCl})_n\text{Na}]^+$  and mixed clusters of these species, e.g.  $[(\text{NaOH})_n(\text{H}_2\text{O})_m\text{Na}]^+$ . These species were also observed by Postberg et al. (2009a) who performed LILBID experiments with pure salt solutions. We find that in this sodium-rich solution the AAs typically form neutral sodiated (sodium-complexed) molecules ( $\text{AA}_{\text{Na}}$ ), in which a sodium ion replaces a hydrogen ion (proton) in the amino acid molecule. This sodiated molecule is cationized by a  $[\text{Na}^+]$  to form a disodiated adduct cation  $[(\text{AA}_{\text{Na}})\text{Na}]^+$  as shown by *His* in Figure 3:



As one proton ( $[H]^+$ ; 1u) is removed and two  $[Na]^+$  (23u) are added, amino acid molecules in a NaCl-rich solution are detectable at masses of AA + 45 u in the mass spectra. The most acidic amino acids (most notably *Asp* and *Glu*) have a characteristic trisodiated peak, in which an additional H is replaced by Na:



This produces an additional molecular peak at AA + 67 u in the mass spectra. One, or both, of these sodiated peaks may occur in an individual spectrum, as illustrated in Table 1. The disodiated and trisodiated peak amplitudes of different amino acids (AA + 45 u and AA + 67 u) vary within an order of magnitude for identical amino acid concentrations. The amino acids are clearly identifiable and in general neither quantitatively nor qualitatively influence the spectral appearance (e.g. peak amplitudes) of the salty matrix solution at the given concentrations (Figure S1).

The only exceptions are sodiated amino acids that may interfere with the ever-present salt-water peaks, e.g. *Arg* + 45 u with  $[(NaCl)_2(NaOH)_2Na]^+$  at m/z 219. Because of a significant peak asymmetry, the mass resolution (600-800 m/ $\Delta$ m) of the spectrometer used for this work is, however, sufficient to resolve interferences of this magnitude, such as the 0.19 u mass difference between *Arg* + 45 u and  $[(NaCl)_2(NaOH)_2Na]^+$  (Figure 4).

Table 1 shows the detection limits of amino acids in salty solutions. The detection limits were individually determined for each amino acid (apart from *Gly*, which

was measured in a mixture) with the experimental parameters (laser intensity and delay time) optimized for greatest sensitivity to the amino acid under investigation. Trisodiated ions of Asp and Glu are detectable at the lowest concentrations in our experimental setup.

### **3.2 Amino acids at abiotic abundances in salty solutions with carboxylic acids (Solution type ii)**

As in the case of Solution type i,  $[(\text{NaOH})_n\text{Na}]^+$ ,  $[(\text{NaCl})_n\text{Na}]^+$  and mixed clusters of these species, e.g.  $[(\text{NaOH})_n(\text{H}_2\text{O})_m\text{Na}]^+$  (Postberg et al., 2009a) from the inorganic spectral background are observable. The characteristic sodiated peaks of *Gly* and *Ala* dominate the other sodiated amino acid peaks in the mass spectrum of the abiotic mix (Figure 5). Despite the low concentrations of the amino acids, the majority can be identified, with *Ser* as the exception. Typical amino acid fragments ( $[\text{NH}_4]^+$ ,  $[\text{CH}_2\text{NH}_2]^+$ ,  $[\text{AA-OH}]^+$ ,  $[\text{AA-NH}_2]^+$  and  $[\text{AA-COOH}]^+$ ), as seen in low salinity solutions (Klenner et al., 2020), or their sodiated forms, are not observable in the spectrum of Solution type ii. If these fragments are indeed produced during laser desorption of this Solution type, they must be present only in very low quantities and/or interfere with more abundant species from the matrix solution. Here we specifically note that the disodiated ( $M + 45$  u) peaks of the most abundant carboxylic acids - valeric acid and methylbutyric acid (molecular weights: 102 u)

at a total concentration of 120 ppmw (considered likely to be detectable) - interfere with a salt species at  $m/z$  147 ( $[(\text{Na}_2\text{CO}_3)(\text{H}_2\text{O})\text{Na}]^+$ ) and are unresolvable with the available mass resolution.

### **3.3 Fatty acids at abiotic and biotic concentration ratios (Solution type iii)**

For comparison with the abiotic concentration ratios used by Klenner et al. (2020) (Figure 6 upper panel), we measured fatty acids (sodium salts - see Methods) at simulated biotic concentration ratios in a water-acetonitrile matrix (50:50 vol) (Figure 6 lower panel). Despite the different abundance ratios of the fatty acids, no indication of peak suppression or matrix effects was found. The deprotonated molecular peak amplitude pattern was found to match that of the abundance ratios of the fatty acids in the original solution, as observed with the abiotic case in Klenner et al. (2020), confirming that no unexpected ion suppression effects on ion formation due to concentration imbalances of the different fatty acids occur. No clear preference in forming particular molecular peak ions was observed, despite the differing molecular masses of the fatty acids. Anions of the form  $[\text{M}-2\text{H}+\text{Na}]^-$ , as seen in e.g. electrospray ionization experiments on dyes (Holcapek et al., 2007), were not found. Chlorinated adducts were also not observed, due to the absence of chlorine in the solution.

Detection limits for the fatty acids used here in a salt poor solution have been previously determined to be  $< 0.02 \mu\text{mol/L}$  ( $< \approx 5 \text{ ppbw}$ ) (Klenner et al., 2020). Additionally, some fatty acids were also tested in a salty solution (0.1 M NaCl). They were not detectable at the solubility limit (about 30 ppmw for hexadecanoic acid).

Sodiated dimers of the form  $[\text{C}_{16,18} + \text{C}_{12,14,16,18,20} - 2\text{H} + \text{Na}]^-$  can be clearly observed from species for which the combined fatty acid concentration exceeds  $\approx 300 \times 10^{-6} \text{ M}$  (Figure 6 lower panel). All dimers are identifiable as one of the fatty acids at the highest concentration of  $275 \times 10^{-6} \text{ M}$ , i.e.  $\text{C}_{16}$  and  $\text{C}_{18}$ , in combination with another even carbon number fatty acid at a concentration of  $55 \times 10^{-6} \text{ M}$  or  $275 \times 10^{-6} \text{ M}$ . The dimers were not observed in the abiotic case because of the lower fatty acid concentrations (each fatty acid at  $5.5 \times 10^{-6} \text{ M}$ ). Non-sodiated dimers were not observed.

There are conspicuous peaks at  $m/z$  172 and  $m/z$  186. The two peaks were also observed by Klenner et al. (2020) in the abiotic case. Although their exact origin is unclear, these peaks are associated with the fatty acid samples (see Discussion).

### **3.4 Complex biotic mix of amino acids and fatty acids (Solution type iv)**

Spectra arising from a low salinity solution of eight amino acids, nine fatty acids and fifteen carboxylic acids together at biotic concentration ratios were measured to simulate a spectrally demanding and complex mixture of organics in water ice grains with embedded biosignatures. Figures 7 and 8 show sections of mass spectra of this type of solution. The mass spectra were recorded in the cation (Figure 7) and anion (Figure 8) modes of the mass spectrometer, respectively.

Amino acids can be identified in such a complex mix by their protonated and deprotonated molecular peaks in the mass spectra, with sodiated species not expected to be observed owing to the low salinity of the background solution. Although the sensitivity of the method varies for different amino acids - reflecting differences in ion formation efficiency and therefore detection thresholds (Klenner et al., 2020) - amino acids other than *Gly* dominate the mass spectra of this biotic mixture. For example, *Arg*, *Asp* and *Lys* show especially high peak amplitudes (Figure 7 and Figure 8). Despite the differences in ion formation efficiency, we easily detect the characteristic spectral signatures, as initially applied to the solution to mimic biotic processes (e.g. Dorn et al., 2011). Extrapolating from the peak amplitudes, all amino acids would still be detectable even if an enrichment factor of 100 would have been chosen instead of 1000 (see 2.2.3). *Arg*, *Asp* and *Lys* would still be easily detectable with an enrichment factor of 10, likely even without any enrichment applied.

Fatty acids can be identified in such a complex mixture by their deprotonated molecular peaks ( $[M-H]^-$ ) in the anion mode (Figure 8). The fatty acid biosignature abundance pattern, as seen in the mixture consisting only of fatty acids at biotic concentrations (Figure 6 bottom panel), is clearly observable and reflects the different biotic fatty acid concentrations. Even carbon number fatty acids are present in much higher abundances than odd carbon number fatty acids, as would be expected from biotic processes (e.g. Dorn et al., 2011). However, a general slight decline in sensitivity with increasing carbon number, due to the increasing poor solubility, can be observed. Extrapolating from the peak amplitudes, all fatty acids would still be detectable even if an enrichment factor of 10 would have been chosen instead of 100 (see section 2.2.3). Even numbered fatty acids would still be easily detectable without any enrichment applied.

Molecular peaks of the background carboxylic acids can also be identified, except decanoic acid (5 ppmw), propionic acid (2 ppmw) and formic acid (2 ppmw), which were present at the lowest concentrations of all background carboxylic acids. We therefore infer these three carboxylic acids to be present in the solution at abundances lower than their respective detection thresholds. Although present in higher concentrations, no interference of these abiotic organic compounds with any of the biogenic signals was observed.

## 4. Discussion

### 4.1 Salt rich amino acid solutions

In this work, for the first time, analogue mass spectra for amino acids potentially captured in salty ice grains from an ocean bearing moon have been investigated. There are some fundamental differences in comparison with the previously investigated (Klenner et al., 2020) cationic mass spectra of amino acids in a salt-poor matrix.

Our results indicate that the protonated molecular peaks, which are strongest in a salt-poor medium, are suppressed (e.g. Piwowar et al., 2009) in the salt-rich case, with the strongest mass spectrometric signals from amino acids in Na-rich ocean water instead arising from sodiated cations (Figures 3 and 5). These appear at masses  $M(\text{olecule}) + 45 \text{ u}$  and  $M + 67 \text{ u}$ , respectively. In these complexes, one or two protons ( $[\text{H}]^+$ ) are replaced by one or two sodium ions in the molecular structure and addition of another  $[\text{Na}]^+$  cation provides a positive charge (Table 1) to the complex. Sodiation of organic molecules in a sodium rich environment is a well-known process in electrospray ionization (ESI) mass spectrometry (e.g. Newton and McLuckey, 2004; Concina et al., 2006). As in ESI, the polysodiated complexes in LILBID are likely to result from the substitution of carboxylic or amidic protons by  $\text{Na}^+$ , with the degree of sodiation dependent on the number of oxygen (from OH) and nitrogen atoms available in the molecule.

As in pure water the sensitivity of the method, and thus the detection limits, varies between different amino acids. The different side chains confer a wide range of properties, with the logarithmic acid dissociation constant  $pK_a$  the most relevant here (e.g. Wu et al., 1992). The more positive the  $pK_a$ , the less dissociation of the acid at any given pH, i.e. the weaker the acid. In pure water, the lowest detection limits are determined to be those for *Arg* and *Lys* (1 nmol/L) - amino acids with basic side chains and relatively high  $pK_a$  values (Klenner et al., 2020). In the salty matrix we found the lowest detection limits (Table 1), those for sodiated *Asp* and *Glu*, to be about 3  $\mu\text{mol/L}$  (compared with about 0.1  $\mu\text{mol/L}$  for the relevant (non-sodiated) peaks in salt poor water). Both amino acids have acidic side chains and relatively low  $pK_a$  values.

In general, sensitivity to those amino acids that have been investigated in both matrices drops between a factor of 2 (*Ser*) and 5 orders of magnitude (*Arg*) when a 1% concentration of sodium salts is present. Experiments on NaCl-rich *Gly* solutions showed that the activity of *Gly* in the *Gly*-NaCl-H<sub>2</sub>O system diminishes with increasing NaCl concentrations giving rise to a so-called salt-in effect for amino acids (Sirbu and Iulian, 2010). We conclude that a high salt concentration also suppresses the characteristic organic peaks in our LILBID experiments. However, sensitivities vary significantly less between different sodiated amino acids (Table 1) compared to the sensitivity variations observed between protonated molecular species in a salt poor matrix (Table 1 in Klenner et al., 2020). The salts

(and  $\text{NH}_3$ ) may function as a pH buffer in the solutions used here and in turn counter pH dependent effects on the different sensitivities to the amino acids and/or the ionic bonding of  $\text{Na}^+$  to the amino acids might be more similar among different molecular structures than protonation of amino acid molecules.

Unlike identical measurements with amino acids at concentrations varying from 50 to 1000 ppmw in pure water (Klenner et al., 2020), in a salty solution no characteristic fragmentation of the amino acids was observed (whether sodiated or not) in the resulting mass spectra. The high salt concentration may have neutralized charged fragments or suppressed the fragmentation process of the organics. In the latter case, although out of the scope of this work, we hypothesize that uncomplexed amino acids may be less stable than the sodium complexes formed in a sufficiently  $[\text{Na}]^+$ -rich solution. This appears to differ from the case of ESI mass spectrometry, in which fragment cations of the form  $[\text{Na}_2\text{NH}_2]^+$ ,  $[\text{NaOCNNa}]^+$ ,  $[\text{Na}_3\text{CN}_2]^+$  can form from sodiated organic molecules, dependent on the elemental composition of the analyzed molecule (Shi et al., 2005).

In Solution type ii, several amino acids and salts, together with 14 carboxylic acids, were measured in the cation mode to simulate a more complex mixture, as might occur in Enceladus' ocean. The goal was to investigate a) interferences between mass lines and b) matrix effects on the sensitivity for amino acids. Indeed, some of the peaks from sodiated amino acids have isobaric masses, at the integer level, with

salt- and salt-water derived peaks. However, the mass difference between these cationic species are relatively large, typically on the order of 0.15 u to 0.2 u (Figure S2), and can be readily resolved with a mass resolution of about  $m/\Delta m = 1000$ . For example, the disodiated *Arg* cation interferes with the salt cluster species  $[(\text{NaCl})_2(\text{NaOH})_2\text{Na}]^+$  at  $m/z$  219. The mass difference of 0.19 u between these two species can be resolved with the laboratory reflectron (mass resolution of  $m/\Delta m = 600\text{-}800$ ) used here (Figure 4).

Although some of the carboxylic acids were present in higher concentrations than most of the amino acids (e.g. valeric acid and methylbutyric acid at concentrations of almost 600  $\mu\text{mol/L}$ ) no sodium complexes involving them were detectable in Solution type ii (cation mode). Their concentrations probably were below their detection limits in a salty matrix. This finding is in agreement with our non-detection of sodiated fatty acids at their solubility limit (approx. 30 ppm for hexadecanoic acid) in a solution with identical salt compounds. They could, however, be identified in the negative mode in a low-salinity solution.

## 4.2 Fatty acids

If present in Enceladus' ocean, the poorly soluble long-chain fatty acids will probably most easily enter the plume within salt-poor ice grains formed from an organic layer at the oceanic surface (Postberg et al., 2018a). Under such conditions,

fatty acids produce characteristic deprotonated molecular peaks in anion mass spectra (Figures 6 and 8) even at trace concentrations of a few tens of nmol/L (Klenner et al., 2020).

In the biotic mixture used for this work, with concentrations differing between fatty acids with even and odd carbon numbers, the peak amplitude pattern again matches that expected from the fatty acid concentrations (Figure 6 and 8). In contrast to amino acids, detection sensitivities vary by only a small amount between fatty acids ranging in size from 12 to 20 carbon atoms, with spectral peaks decreasing only slightly for identical concentrations with increasing carbon number. This reflects the fact that, in contrast to amino acids, the fatty acids have very similar structures and  $pK_a$  values. This similarity enables the facile distinction between biotic and abiotic abundance patterns.

Even at low to intermediate sodium concentration in the solution ( $\sim 0.75$  mmol/L from the sodium salts used), sodiated dimers of the fatty acids are observed (Figure 6), with amplitudes approximately two orders of magnitude lower than those of the deprotonated molecular peaks. A combined fatty acid concentration for two species of  $\approx 300$   $\mu\text{mol/L}$  is sufficient to create very clear dimer signals at the given  $[\text{Na}]^+$  concentration and, extrapolating from the observed amplitudes (Figure 6), concentrations of  $100$   $\mu\text{mol/L}$  should still allow for a dimer detection. With increasing salinity the sodiated dimers are likely to become more abundant than the

deprotonated molecular anions, which may suffer from similar suppression effects as observed in the case of amino acids.

There are conspicuous peaks at  $m/z$  172 and  $m/z$  186 in all fatty acid mass spectra. These two peaks are also observed by Klenner et al. (2020). The exact origin of these peaks is still unclear, but they are undoubtedly associated with the fatty acid samples. They may potentially be fragments due to  $C_nH_{2n}$  cleavage from the fatty acids in combination with electron capture ionization. The peaks could also represent undefined sodiated species. However, the most likely possibility is that the peaks derive from a specific but currently unknown contamination of the fatty acid sodium salts. For more details about the potential origin of these peaks, see Klenner et al. (2020).

### **4.3 Complex biosignature mixtures**

Two scenarios were investigated. The first (Solution type ii) simulated spectra arising from amino acids at putative abiotic abundances together with other abiotic organic compounds with added salts that are representative of Enceladus' ocean composition. These were measured in the cation mode of the mass spectrometer. In the second scenario (Solution type iv), we investigated spectra generated by biotic concentrations of fatty acids and amino acids in ice grains as may form from a putative organic film on the surface of Enceladus' ocean. For the amino acids, biotic

concentration ratios as they appear in Earth's ocean were used and enrichment factors inferred from similar processes on Earth's ocean then applied (section 2.2.3). The availability of amino acids in Enceladus' ocean probably differs from that in Earth's ocean. However, as the most well-characterized, cold water, salty environment in which life flourishes, Earth's ocean currently represents the only example from which biotic amino acid abundance ratios can be derived for application to Enceladus. As in Solution type ii, a large number of potential abiotic organics were included in the simulant mixture. These parameters can be expected to produce the most complex, and therefore challenging, mass spectra for a biotic case. These spectra were obtained using both positive and negative modes.

In both scenarios the abiotic and biotic mass spectrometric fingerprints of the biosignatures could be successfully identified (Figures 5, 7 and 8). No unresolvable interferences with any of the amino acids and fatty acids in the solutions were observed. In the analytically demanding salty solutions, sodiated amino acids can be identified down to approximately 1 ppmw. The non-detection of *Ser* does, however, indicate that due to matrix effects the detection limits are slightly higher in comparison with those for a solution with just individual amino acids. In the salt-poor solution the sensitivity to amino acids is much higher in most cases, as expected from the results by Klenner et al. (2020). There, 500 ppbw concentrations of *Arg*, and *Lys* created very clear signals (signal to noise ratio  $\approx 50$  sigma for both

amino acids) in the cation mode (Figure 7) while *Asp* and *Ser* are the dominant amino acid signals in the anion mass spectra (Figure 8).

In a similar way spectra of fatty acid mixtures at biotic concentrations down to 100 ppbw reflect the biotic abundance pattern in which even carbon number fatty acids are clearly more abundant than odd carbon number fatty acids, even in a complex mixture where different organics could theoretically easily interfere with each other (Figure 8). However, a stronger dependence on the number of carbon atoms (i.e. C-number) was observed when compared to Solution type iii (Figure 6), with decreasing sensitivity towards higher carbon numbers. Extrapolating from the observed amplitudes, the biotic patterns would have been clearly identifiable in the mass spectra even at 10 – 100 times reduced concentrations in agreement with the detection limits found by Klenner et al. (2020).

Klenner et al. (2019) showed that the experimental parameters of the LILBID analogue setup can be correlated with impact speeds of ice grains onto impact ionization mass spectrometer targets in space. By comparison between the experimental parameters used here (intermediate to high laser intensities and intermediate to high delay times) with amino acids and those required to simulate different impact speeds of the ice grains, we infer that instrument sensitivity to amino acids in grains formed from a salty ocean environment is maximized at impact speeds of 5 – 10 km/s. The slightly higher values compared to those in pure

water agree with the observation that the sodiated amino acids, which are the characteristic peaks in a salty environment, resist fragmentation more than the protonated and deprotonated molecular species produced in a salt-poor matrix. We confirm the finding of Klenner et al. (2020) that using very high delay times and intermediate laser intensities, equivalent to impact speeds of 3 – 6 km/s, maximizes the detection sensitivity for fatty acids.

Previous work has shown that organics (both refractory and volatile) in projectiles are capable of surviving the impact process at velocities of up to 5 km/s (e.g. Burchell et al., 2014; Bowden et al., 2009; New et al., 2020). Further experiments, in which capsules containing aqueous amino acid solutions were subjected to impacts of steel projectiles at up to ~2 km/s, showed that a large fraction (40-70 %) of the amino acids also survived (Blank et al., 2001). In the specific case of ice grains, modelling of particle impacts onto aluminum targets indicates that at relative velocities of up to 5 km/s, comparable with Enceladus plume transect velocities, little to no thermal degradation of entrained organics, such as amino acids, should occur (Mathies et al., 2017).

The LILBID technique is known to be capable of preserving and measuring delicate organic structures, such as intact membrane complexes (Morgner et al., 2007), as a function of applied laser intensity, with ultra-soft ionization occurring at low laser energies. However, the results presented in this work, and those of Klenner et al.

(2020), use higher laser energies which are typically more destructive, and yet show that a detectable fraction of organic molecules, in particular amino acids, fatty acids and peptides, survive at equivalent impact speeds of  $> 5$  km/s. The fragmentation of organic macromolecules during impacts of ice grains from Enceladus (Postberg et al. 2018a) shows similar behavior, with the characteristic (70 – 200 u) spectral signatures of the breakup of large ( $m > 200$  u) parent molecules only becoming detectable at impact speeds above 5 km/s and becoming more prominent at speeds  $> 10$  km/s (Postberg et al. 2018a).

These laboratory and flight results are in good agreement with ab initio molecular dynamics simulations which show that even a few layers of water ice molecules can effectively protect organic molecules from impact fragmentation (Jaramillo-Botero et al., under review). With ionization also promoted by a liquid or frozen water matrix (Wiederschein et al. 2015), the survivability and detectability of organics appears to be significantly improved in ice grains ejected into space by ocean-bearing moons, even if encountered at relative velocities above 5 km/s.

These relative speeds are of keen interest for feasibility studies of flying through the plume of Enceladus on ballistic trajectories. Cassini flew through the plume at speeds as low as 7.5 km/s, but plume transects at 4-5 km/s are possible (Reh et al, 2016; Mitri et al., 2018). Even slower speeds can be achieved, but grain impact speeds of greater than approximately 3 km/s were required to generate sufficient

ionization for the analysis of plume material with Cassini's CDA. Thus not only are plume transects below 3 km/s undesirable for this technique, but based on our work they also provide no improvements to the diagnostic capability of the mass spectrometry.

## **5. Conclusions**

The proven ability of the LILBID experiment to simulate the impact ionization mass spectra of water ice dominated grains (e.g. Postberg et al., 2009a, 2011a, 2018a; Khawaja et al., 2019; Klenner et al., 2019) has been applied to the simulation of ice grains containing biosignatures in biotic and abiotic concentration ratios. Potentially abiotic organic substances (such as simple carboxylic acids) and inorganic substances (salts and ammonia) have been added to investigate detection limits, potential mass spectral interferences and suppression effects, with the aim of verifying whether abiotic and biotic spectral fingerprints can be clearly identified under complex conditions. A more precise quantitative determination of the biosignatures (e.g. calibration curves), however, is beyond the scope of this paper and will be a goal of future work.

Enceladus' organics are principally thought to enter ice grains either from a solution in the ocean or from an organic layer on top of the ocean. While poorly soluble compounds can only originate from that layer and will be part of salt-poor ice grains

(Type 2; Postberg et al., 2018a; Khawaja et al., 2019), organics with higher water solubility will also be incorporated into ice grains forming from salty ocean droplets (Type 3; Postberg et al., 2009a). If present, free amino acids will be dissolved in the Enceladean ocean and are thus expected also to be found in salt-rich ice grains. All tested amino acids form sodiated cations which produce the most intense amino acids signal by far under these conditions. To discriminate between the characteristic sodiated mass peaks of amino acids and other dissolved organic species and extraneous peaks from near isobaric salt species, a future flight instrument will require a mass resolution of at least  $m/\Delta m = 700$ , and ideally  $m/\Delta m > 1000$ .

Amino acids generally favor forming cations whereas fatty acids favor forming anions. A future flight instrument therefore ideally needs to be capable of detecting both cations and anions to cover the complete range of biosignatures investigated here.

Of the amino acids tested, *Asp* and *Glu*, via their sodium-complexes, have been detected at the lowest concentrations (0.5 ppmw). Fatty acids and other carboxylic acids are not detected in such a high salinity environment at or below a level of 50 ppmw. In an environment of intermediate salinity sodiated dimers of fatty acids, however, can be detected at a level of 0.1 mmol/L, equivalent to ~25 ppmw. By contrast, deprotonated anions from fatty acids and protonated cations from amino

acids will dominate spectra from salt-poor water ices and are detectable down to the nanomolar or ppbw level, respectively (Klenner et al., 2020).

It is reasonable to assume that the observed suppression and complexation effects arising from interaction with the salty matrix will also affect other organic species. Recently identified soluble organic compounds, found in many salt-poor Type 2 grains, are believed to enter grains via condensation from the vapor phase (Khawaja et al., 2019). Such soluble organics should then also be incorporated into ocean spray, which is thought to form salty Type 3 ice grains rising through the Enceladus fractures (Postberg et al. 2009a, 2011a). The work presented here, however, indicates that the detection and identification of such compounds in spectra generated by impacts of salty Type 3 grains might be more difficult than for the salt-poor grains.

The initial abundances of amino acids and fatty acids at given concentrations are reflected in the amplitudes of their molecular peaks, including the sodiated molecular peaks of amino acids in salty solutions. Abiotic and biotic fatty acid signatures within the ice grains are easily discernible. The ratios of various amino acids to *Gly* and the odd-even carbon number abundance pattern of fatty acids serve as biosignatures that can be readily distinguished from each other in mass spectra, even under demanding matrix conditions in a salt poor as well as a salt rich environment. Should they be present, these key organic species and their

abiotic/biotic signatures are therefore likely to be identifiable in impact ionization mass spectra from ice grains recorded in space. Detection limits for space instrumentation with more efficient ion detectors and higher dynamic ranges than the experimental setup used here may be expected to be at least two orders of magnitude lower than the values reported here and in Klenner et al. (2020). We conclude that in a salt-poor water ice matrix, all investigated biosignatures could then be detectable as such down to the nanomolar level, with amino acids in a salty environment detectable down to at least the micromolar level.

To simulate biotic concentrations, we used values from the only example we have: Earth's ocean. The concentrations and specific types of fatty acids and amino acids in an inhabited extraterrestrial environment will almost certainly be very different. Although our results demonstrate the ability to identify by using LILBID a large number of biogenic tracers at Earth-like concentrations, it is impossible to say whether this or any other method will be able to detect the concentrations of these substances in ice grains from an extraterrestrial ocean world.

It is important to note, however, that according to recent work by Truong et al. (2019), concentrations of abiotic amino acids may be expected to be barely detectable. Specifically, aspartic acid and arginine have been shown to decompose within thousands, to at most a few million years in oceanic water and any detection of these compounds in material from ocean worlds will be strong evidence for a

very efficient, probably extant generation mechanism. Another study implies high compatibility of amino acids in ice Ih during the freezing of an aqueous solution and suggests that the ice matrix protects amino acids from decomposition or racemization (Hao et al. 2018). The LILBID experiments conducted so far (this work, and Klenner et al., 2020) show that such compounds can be reliably detected and identified at low concentrations, particularly arginine in a salt-poor matrix and aspartic acid in a salt-rich matrix.

In the future, the LILBID technique will be used to perform quantitative investigations of not only the biosignatures discussed in this work, but also a wide range of other relevant organic compounds, in matrices designed to mimic ice grains derived from a range of realistic oceanic compositions for Enceladus and Europa. LILBID experiments on DNA extracted from bacterial cultures, as well as lysed and disrupted cellular material, are currently underway to investigate the mass spectral appearance of these biological materials after simulated impact ionization.

The results of this work also aid future space mission planning, with laboratory experimental parameters used to derive recommended impact velocity regimes and instrument configurations (Klenner et al., 2019) - for ice grain impacts onto spaceborne mass spectrometers - which maximize the chances of detecting biomarker compounds.

The survivability of organics appears to be significantly improved when large molecules are protected by a liquid or frozen water matrix, which at the same time promotes ionization (Wiederschein et al., 2015). Using impact ionization mass spectrometers, the efficient detection of amino acids and fatty acids in ice grains present in plumes or ejecta emitted from Enceladus and Europa, and the reliable identification of abiotic and biotic signatures of these organics is found to occur at encounter velocities of 3 – 8 km/s, with an optimal window at 4 - 6 km/s. At these speeds, in a water-rich matrix, even complex organic molecules remain largely intact, yet are expected to efficiently form cations and anions from impact ionization, yielding the highest possible signal-to-noise ratio. This means that ballistic fly-throughs of the Enceladus plume (and potential plumes of other ocean worlds) at these velocities will yield optimal diagnostic data on the presence and identity of potential biogenic compounds.

### **Acknowledgements**

The authors thank Lenz Nölle for valuable discussions about the experimental results and Marie Dannenmann for discussions about future studies. The research leading to these results received funding from the German Research Foundation (DFG) projects PO 1015/2-1, /3-1, /4-1, project AB 63/9-1 and from the European Research Council (ERC) under the European Union's Horizon 2020 research and

innovation programme (ERC Consolidator Grant 724908-Habitat OASIS). JIL was supported by the Distinguished Visiting Scientist Program at the NASA Jet Propulsion Laboratory during the course of the work. Most of this work was carried out at the Institute of Earth Sciences, Heidelberg University. Some additional work was carried out at the Wilhelm-Ostwald-Institute, Leipzig University, and at the Jet Propulsion Laboratory, California Institute of Technology, under a contract with the National Aeronautics and Space Administration.

#### **Author Disclosure Statement**

No competing financial interests exist.

#### **References**

Altwegg, K., Balsiger, H., Bar-Nun, A., Berthelier, J.J., Bieler, A., Bochsler, P., Briois, C., Calmonte, U., Combi, M.R., Cottin, H., De Keyser, J., Dhooghe, F., Fiethe, B., Fuselier, S.A., Gasc, C., Gombosi, T.I., Hansen, K.C., Haessig, M., Jäckel, A., Kopp, E., Korth, A., Le Roy, K., Mall, U., Marty, B., Mousis, O., Owen, T., Rème, H., Rubin, M., Sémon, T., Tzou, C.Y., Waite, J.H., and Wurz, P. (2016) Prebiotic chemicals-amino acid and phosphorus-in the coma of comet 67P/Churyumov-Gerasimenko. *Sci Adv* 2:e1600285.

Annesley, T.M. (2003) Ion Suppression in Mass Spectrometry. *Clin Chem* 49:1041-1044.

Berg, J.M., Tymoczko, J.L., and Stryer, L. (2012) Fatty Acid Metabolism. In *Biochemistry*, W. H. Freeman New York, p 1050.

Blank, J.G., Miller, G.H., Ahrens, M.J., and Winans, R.E. (2001) Experimental shock chemistry of aqueous amino acid solutions and the cometary delivery of prebiotic compounds. *Orig Life Evol Bios* 31:15-51.

Bowden, S.A., Parnell, J., and Burchell, M.J. (2009) Survival of organic compounds in ejecta from hypervelocity impacts on ice. *Int J Astrobiol* 8:19-25.

Bouquet, A., Glein, C.R., and Waite, J.H. (2019) How Adsorption Affects the Gas-Ice Partitioning of Organics Erupted from Enceladus. *Astrophys J* 873:13pp.

Burchell, M.J., Bowden, S.A., Cole, M., Price, M.C., and Parnell, J. (2014) Survival of Organic Materials in Hypervelocity Impacts of Ice on Sand, Ice, and Water in the Laboratory. *Astrobiology* 14:473-485.

Burrows, S.M., Ogunro, O., Frossard, A.A., Russel, L.M., Rasch, P.J., and Elliot S.M. (2014) A physically based framework for modeling the organic fractionation of sea spray aerosol from bubble film Langmuir equilibria. *Atmos Chem Phys* 14:13601-13629.

Choblet, G., Tobie, G., Sotin, C., Behouňková, M., Cadek, O., Postberg, F., and Soucek, O. (2017) Powering prolonged hydrothermal activity inside Enceladus. *Nat Astron* 1:841-847.

Concina, B., Hvelplund, P., Nielsen, A.B., Brøndsted Nielsen, S., Rangama, J., Liu, B., and Tomita, S. (2006) Formation and Stability of Charged Amino Acid Clusters and the Role of Chirality. *J Am Soc Mass Spectrom* 17:275-279.

Creamer, J.S., Mora, M.F., and Willis P.A. (2017) Enhanced Resolution of Chiral Amino Acids with Capillary Electrophoresis for Biosignature Detection in Extraterrestrial Samples. *Anal Chem* 89:1329–1337.

Cronin J.R. and Pizzarello, S. (1983) Amino acids in meteorites. *Adv Space Res* 3:5–18.

Davila A.F. and McKay C.P. (2014) Chance and Necessity in Biochemistry: Implications for the Search for Extraterrestrial Biomarkers in Earth-like Environments. *Astrobiology* 14:534–540.

Dorn, E.D., Nealson K.H., and Adami, C. (2011) Monomer abundance distribution patterns as a universal biosignature: Examples from terrestrial and digital life. *J Mol Evol* 72:283–295.

Dunn, M.S., Ross, F.J., and Read, L.S. (1933) The Solubility of the Amino Acids in Water. *J Biol Chem* 103:579-595.

Georgiou, C.D. and Deamer, D.W. (2014) Lipids as Universal Biomarkers of Extraterrestrial Life. *Astrobiology* 14:541–549.

Glavin D.P., Callahan, M.P., Dworkin, J.P., and Elsila, J.E (2011). The effects of parent body processes on amino acids in carbonaceous chondrites. *Meteorit Planet Sci* 45:1948-1972.

Glein, C.R., Baross, J.A., and Waite, J.H. (2015) The pH of Enceladus' ocean. *Geochim Cosmochim Acta* 162:202-219.

Glein, C.R., Postberg, F., and Vance, S. (2018) The Geochemistry of Enceladus: Composition and Controls. In *Enceladus and the Icy Moons of Saturn*, University of Arizona Press, pp 39-56.

Glein, C.R., and Waite, J.H. (2020) The Carbonate Geochemistry of Enceladus' Ocean. *Geophys Res Lett* 47: e2019GL085885.

Goldstein, D.B., Hedman, M., Manga, M., Perry, M., Spitale, J., and Teolis, B. (2018) Enceladus Plume Dynamics: From Surface to Space. In *Enceladus and the Icy Moons of Saturn*, University of Arizona Press, pp 175-194.

Hand, K.P., Carlson, R.W., and Chyba, C.F. (2007) Energy, Chemical Disequilibrium, and Geological Constraints on Europa. *Astrobiology* 7:1006-1022.

Hao, J., Giovenco, E., Pedreira-Segade, U., Montagnac, G., and Daniel, I. (2018) Compatibility of Amino Acids in Ice Ih: Implications for the Origin of Life. *Astrobiology* 18:381-392.

Hayes, J.M. (1967) Organic constituents of meteorites – A review. *Geochim Cosmochim Acta* 31:1395-1440.

Higgs P.G. and Pudritz R.E. (2009) A thermodynamic basis for prebiotic amino acid synthesis and the nature of the first genetic code. *Astrobiology* 9:483–490.

Hillier, J.K., Green, S.F., McBride, N., Schwanethal, J.P., Postberg, F., Srama, R., Kempf, S., Moragas-Klostermeyer, G., McDonnell, J.A.M., and Grün, E. (2007) The composition of Saturn's E ring. *Mon Not R Astron Soc* 377:1588-1596.

Holcapek, M., Volná, K., and Vanerková, D. (2007) Effects of functional groups on the fragmentation of dyes in electrospray and atmospheric pressure chemical ionization mass spectra. *Dyes and Pigments* 75:156-165.

Hsu, H.-W., Postberg, F., Sekine, Y., Shibuya, T., Kempf, S., Horányi, M., Juhász, A., Altobelli, N., Suzuki, K., Masaki, Y., Kuwatani, T., Tachibana, Sirono, S.-I., Moragas-Klostermeyer, G., and Srama, R. (2015) Ongoing hydrothermal activities within Enceladus. *Nature* 519:207-210.

Huang, Y., Wang, Y., Alexandre, M.R., Lee, T., Rose-Petruck, C., Fuller, M., and Pizzarello, S. (2005) Molecular and compound-specific isotopic characterization of

monocarboxylic acids in carbonaceous meteorites. *Geochim Cosmochim Acta* 69:1073-1084.

Huybrighs, H.L.F., Roussos, E., Blöcker, A., Krupp, N., Futaana, Y., Barabash, S., Hadid, L.Z., Holmberg, M.K.G., Lomax, O., and Witasse, O. (2020) An Active Plume Eruption on Europa During Galileo Flyby E26 as Indicated by Energetic Proton Depletions. *Geophys Res Lett* 47: e2020GL087806.

Jaramillo-Botero, A., Cable, M., Hofmann, A., Hodyss, R., Malaska, M., and Lunine, J. Understanding hypervelocity sampling of biosignatures in space missions. *Astrobiology*: under review.

Jia, X., Kivelson, M.G., Khurana K.K., and Kurth W.S. (2018) Evidence of a plume on Europa from Galileo magnetic and plasma wave signatures. *Nat Astron* 2:459–464.

Karas, M, Bahr, U., Ingendoh, A., Nordhoff, E., Stahl, B., Strupat, K., and Hillenkamp, F. (1990) Principles and applications of matrix-assisted UV-laser desorption/ionization mass spectrometry. *Anal Chim Acta* 241:175-185.

Karas, M., Bahr, U., Ingendoh, A., Nordhoff, E., Stahl, B., Strupat, K., and Hillenkamp F. (1991) Principles and applications of matrix-assisted UV-laser desorption/ionization mass spectrometry. *J Chromatogr B* 562:745-746.

Karas, M., Glückmann, M., and Schäfer J. (2000) Ionization in matrix-assisted laser desorption/ionization: singly charged molecular ions are the lucky survivors. *J Mass Spectrom* 35:1-12.

Kawahata, H., and Ishizuka, T. (1992) Amino acids in interstitial waters from sites 790 and 791 in the Izu-Bonin island arc. In Proc. ODP, Sci. Results, 126, College Station, TX (Ocean Drilling Program), pp 531-540.

Kempf, S., Altobelli, N., Briois, C., Grün, E., Horanyi, M., Postberg, F., Schmidt, J., Srama, R., Sternovsky, Z., Tobie, G., and Zolotov, M. (2014) SUDA: A Dust Mass Spectrometer for Compositional Surface Mapping for a Mission to Europa. *European Planetary Science Congress 9:EPSC2014-229*.

Khawaja, N., Postberg, F., Hillier, J., Klenner, F., Kempf, S., Nölle, L., Reviol, R., Zou, Z., and Srama, R. (2019) Low-mass nitrogen-, oxygen-bearing, and aromatic compounds in Enceladean ice grains. *Mon Not R Astron Soc* 489:5231-5243.

Klenner, F., Postberg, F., Hillier, J., Khawaja, N., Reviol, R., Srama, R., Abel, B., Stolz, F., and Kempf, S. (2019) Analogue spectra for impact ionization mass spectra of water ice grains obtained at different impact speeds in space. *Rapid Commun Mass Spectrom* 33:1751-1760.

Klenner, F., Postberg, F., Hillier, J., Khawaja, N., Reviol, R., Stolz, F., Cable, M.L., Abel, B., and Nölle, L. (2020) Analog Experiments for the Identification of Trace

Biosignatures in Ice Grains from Extraterrestrial Ocean Worlds. *Astrobiology* 20:179-189.

Lai, J.C.-Y., Pearce, B.K.D., Pudritz, R.E., and Lee, D. (2019) Meteoritic abundances of fatty acids and potential reaction pathways in planetesimals. *Icarus* 319:685-700.

Loison, A., Dubant, S., Adam, P., and Albrecht, P. (2010) Elucidation of an Iterative Process of Carbon-Carbon Bond Formation of Prebiotic Significance. *Astrobiology* 10:973-988.

Lunine, J., Waite, J.H., Postberg, F., Spilker, L., and Clark, K. (2015) Enceladus Life Finder: The Search for Life in a Habitable Moon. *46<sup>th</sup> Lunar and Planetary Science Conference*: 1525.

Mathies, R.A., Razu, M.E., Kim, J., Stockton, A.M., Turin, P., and Butterworth, A. (2017) Feasibility of Detecting Bioorganic Compounds in Enceladus Plumes with the Enceladus Organic Analyzer. *Astrobiology* 17:902-912.

McKay, C.P., Davila, A., Glein C.R., Hand, K.P., and Stockton, A. (2018) Enceladus Astrobiology, Habitability, and the Origin of Life. In *Enceladus and the Icy Moons of Saturn*, University of Arizona Press, pp 437-452.

Menez, B., Pisapia, C., Andreani, M., Jamme, F., Vanbellinghen, Q.P., Brunelle, A., Richard, L., Dumas, P., and Refregiers, M. (2018) Abiotic Synthesis of Amino Acids in the recesses of the Oceanic lithosphere. *Nature* 564:59–63.

Mitri, G., Postberg, F., Soderblom, J.M., Wurz, P., Tortora, P., Abel, B., Barnes, J.W., Berga, M., Carrasco, N., Coustenis, A., de Vera, J.P.P., D'Ottavio, A., Ferri, F., Hayes, A.G., Hayne, P.O., Hillier, J.K., Kempf, S., Lebreton, J.-P., Lorenz, R.D., Martelli, A., Orosei, R., Petropoulos, A.E., Reh, K., Schmidt, J., Sotin, C., Srama, R., Tobie, G., Vorburger, A., Vuitton, V., Wong, A., and Zannoni, M. (2018) Explorer of Enceladus and Titan (E<sup>2</sup>T): Investigating ocean worlds' evolution and habitability in the solar system. *Planet Space Sci* 155:73-90.

Morgner, N., Kleinschroth, T., Barth, H.-D., Ludwig, B., and Brutschy, B. (2007) A Novel Approach to Analyze Membrane Proteins by Laser Mass Spectrometry: From Protein Subunits to the Integral Complex. *J Am Soc Mass Spectrom* 18:1429-1438.

New, J.S., Mathies, R.A., Price, M.C., Cole, M.J., Golozar, M., Spathis, V., Burchell, M.J., and Butterworth, A.L. (2020) Characterizing organic particle impacts on inert metal surfaces: Foundations for capturing organic molecules during hypervelocity transits of Enceladus plumes. *Meteorit Planet Sci*:1-15.

Newton, K.A., McLuckey, S.A. (2004) Generation and manipulation of sodium cationized peptides in the gas phase. *J Am Soc Mass Spectrom* 15:607-615.

Paganini, L., Villanueva, G.L., Roth, L., Mandell, A.M., Hurford, T.A., Retherford, K.D., and Mumma, M.J. (2019) A measurement of water vapour amid a largely quiescent environment on Europa. *Nat Astron* (in press).

Piwowar, A.M., Lockyer, N.P., Vickerman, J.C. (2009) Salt Effects on Ion Formation in Desorption Mass Spectrometry: An Investigation into the Role of Alkali Chlorides on Peak Suppression in Time-of-Flight-Secondary Ion Mass Spectrometry. *Anal Chem* 81:1040-1048.

Pizzarello, S., Schrader, D.L., Monroe, A.A., and Lauretta, D.S. (2012) Large enantiomeric excesses in primitive meteorites and the diverse effects of water in cosmochemical evolution. *Proc Natl Acad Sci* 109:11949-11954.

Porco, C. C., Dones, L., Mitchell, C. (2017) Could it be snowing microbes on Enceladus? Assessing Conditions in its plume and implications for future missions. *Astrobiology* 17, 876-901.

Postberg, F., Kempf, S., Hillier, J.K., Srama, R., Green, S.F., McBride, N., and Grün, E. (2008) The E-ring in the vicinity of Enceladus II. Probing the moon's interior—The composition of E-ring particles. *Icarus* 193:438-454.

Postberg, F., Kempf, S., Schmidt, J., Brilliantov, N., Beinsen, A., Abel, B., Buck, U., and Srama, R. (2009a) Sodium salts in E-ring ice grains from an ocean below the surface of Enceladus. *Nature* 459:1098-1101.

Postberg, F., Kempf, S., Rost, D., Stephan, T., Srama, R., Trieloff, M., Mocker, A., and Goerlich, N. (2009b) Discriminating contamination from particle components in spectra of Cassini's dust detector CDA. *Planet Space Sci* 57:1359-1374.

Postberg, F., Khawaja, N., Abel, B., Choblet, G., Glein, C.R., Gudipati, M.S., Henderson, B.L., Hsu, H.-W., Kempf, S., Klenner, F., Moragas-Klostermeyer, G., Magee, B., Nölle, L., Perry, M., Reviol, R., Schmidt, J., Srama, R., Stolz, F., Tobie, G., Trieloff, M., and Waite, J.H. (2018a) Macromolecular organic compounds from the depths of Enceladus. *Nature* 558:564-568.

Postberg, F., Schmidt, J., Hillier, J., Kempf, S., and Srama, R. (2011a) A salt-water reservoir as the source of a compositionally stratified plume on Enceladus. *Nature* 474:620-622.

Postberg, F., Grün, E., Horanyi, M., Kempf S., Krüger, H., Schmidt, J., Spahn, F., Srama, R., Sternovsky, Z., and Trieloff, M. (2011b) Compositional Mapping of Planetary Moons by Mass Spectrometry of Dust Ejecta. *Planet Space Sci* 59:1815–1825.

Postberg, F., Clark, R.N., Hansen, C.J., Coates, A.J., Dalle Ore, C.M., Scipioni, F., Hedman, M.M., and Waite, J.H. (2018b) Plume and Surface Composition of Enceladus. In *Enceladus and the Icy Moons of Saturn*, University of Arizona Press, pp 129-162.

Reh, K., Cable, M., Clark, K., Lunine, J., Postberg, F., Spilker, L., and Waite, J.H. (2016) Enceladus Life Finder: The Search for Life in a Habitable Moon. *IEEE Aerospace Conference*, DOI 10.1109/AERO.2016.7500813.

Repeta, D.J. (2014) Chemical Characterization and Cycling of Dissolved Organic Matter. In *Biogeochemistry of Marine Dissolved Organic Matter*, Academic Press Elsevier, pp 21-63.

Roth, L., Saur, J., Retherford, K.D., Strobel, D.F., Feldman, P.D., McGrath, M.A. and Nimmo, F. (2014) Transient Water Vapor at Europa's South Pole. *Science* 343:171-174.

Russel, L.M., Hawkins, L.N., Frossard, A.A., Quinn, P.K., and Bates, T.S. (2010) Carbohydrate-like composition of submicron atmospheric particles and their production from ocean bubble bursting. *Proc Natl Acad Sci USA* 107:6652-6657.

Sekine, Y., Shibuya, T., Postberg, F., Hsu, H.-W., Suzuki, K., Masaki, Y., Kuwatani, T., Mori, M., Hong, P.K., Yoshizaki, M., Tachibana, S., and Sirono, S.-i. (2015) High-temperature water-rock interactions and hydrothermal environments in the chondrite-like core of Enceladus. *Nat Commun* 6:8604 (8pp).

Sherwood, B. (2016) Strategic map for exploring the ocean-world Enceladus. *Acta Astronaut* 126:52-58.

Shi, T., Zhao, J., Shek, P.I., Hopkinson, A.C., and Siu, K.M. (2005) Carbonate, carbamate, urea, and guanidine as model species for functional groups in biological molecules – A combined density functional theory and mass spectrometry examination of polysodiation and gas-phase dissociation. *Can J Chem* 83:1941-1952.

Sirbu, F. and Iulian, O. (2010) The mixing effect of glycine with sodium chloride from activity coefficients investigations at  $T = (303.15 \text{ and } 313.15) \text{ K}$ . *J Optoelectron Adv M* 12:1200-1205.

Sparks, W.B., Hand, K. P., McGrath, M.A., Bergeron, E., Cracraft, M., and Deustua S.E. (2016) Probing for evidence of plumes on Europa with HST/STIS. *Astrophys J* 829:121 (21pp).

Sparks, W.B., Schmidt, B.E., McGrath, M.A., Hand, K.P., Spencer, J.R., Cracraft, M., and Deustua, S.E. (2017) Active cryovolcanism on Europa? *Astrophys J Lett* 839:L18 (5pp).

Spencer, J.R., Nimmo, F., Ingersoll, A.P., Hurford, T.A., Kite, E.S., Rhoden, A.R., Schmidt, J., and Howett, C.J.A. (2018) Plume Origins and Plumbing: From Ocean to Surface. In *Enceladus and the Icy Moons of Saturn*, University Arizona Press, pp 163-174.

Srama, R., Ahrens, T.J., Altobelli, N., Auer, S., Bradley, J.G., Burton, M., Dikarev, V.V., Economou, T., Fechtig, H., Görlich, M., Grande, M., Graps, A., Grün, E., Havnes, O., Helfert, S., Horanyi, M., Igenbergs, E., Jessberger, E.K., Johnson, T.V., Kempf, S., Krivov, A.V., Krüger, H., Mocker-Ahlreep, A., Moragas-Klostermeyer, G., Lamy, P., Landgraf, M., Linkert, D., Linkert, G., Lura, F., McDonnell, J.A.M., Möhlmann, D., Morfill, G.E., Müller, M., Roy, M., Schäfer, G., Schlotzhauer, G., Schwehm, G.H., Spahn, F., Stübig, M., Svestka, J., Tschernjawski, V., Tuzzolino, A.J., Wäsch, R., and Zook, H.A. (2004) The Cassini Cosmic Dust Analyzer. *Space Sci Rev* 114:465-518.

Srama, R., Postberg, F., Henkel, H., Klopfer, T., Li, Y., Simolka, J., Bugiel, S., Kempf, S., Hillier, J., Khawaja, N., Trieloff, M., Abel, B., Moragas-Klostermeyer, G., Strack, H., Schmidt, J., Soja, R., Sternovsky, Z., and Spohn, T. (2015) Enceladus Icy Jet Analyzer (ENIJA): Search for life with a high resolution TOF-MS for in situ characterization of high dust density regions. *EPSC Abstracts* 10:EPSC2015-769.

Summons, R.E., Albrecht, P., McDonald, G., Moldowan, J.M. (2008) Molecular Biosignatures. *Space Sci Rev* 135:133-159.

Taubner, R.-S., Olsson-Francis, K., Vance, S.D., Ramkissoon, N.K., Postberg, F., de Vera, J.-P., Antunes, A., Camprubi Casas, E., Sekine, Y., Noack, L., Barge, L., Goodman, J., Jebbar, M., Journaux, B., Karatekin, Ö., Klenner, F., Rabbow, E.,

Rettberg, P., Rückriemen-Bez, T., Saur, J., Shibuya, T., and Soderlund, K.M. (2020) Experimental and Simulation Efforts in the Astrobiological Exploration of Exooceans. *Space Sci Rev* 216:9.

Trumbo, S.K., Brown, M.E., and Hand, K.P. (2019) Sodium chloride on the surface of Europa. *Sci Adv.* 5:eaaw7123.

Truong, N., Monroe, A.A., Glein, C.R., Anbar, A.D., and Lunine, J.I. (2019) Decomposition of Amino Acids in Water with Application to In-Situ Measurements of Enceladus, Europa and Other Hydrothermally Active Icy Ocean Worlds. *Icarus* 329:140-147.

Waller, S.E., Belousov, A., Kidd, R.D., Nikolic, D., Madzunkov, S.M., Wiley, J.S., and Darrach, M.R. (2019) Chemical Ionization Mass Spectrometry: Applications for the In Situ Measurements of Nonvolatile Organics at Ocean Worlds. *Astrobiology* 19:1196-1210.

Waite, J.H., Glein, C.R., Perryman, R.S., Teolis, B.D., Magee, B.A., Miller, G., Grimes, J., Perry, M.E., Miller, K.E., Bouquet, A., Lunine, J.I., Brockwell, T., and Bolton, S.J. (2017) Cassini finds molecular hydrogen in the Enceladus plume: Evidence for hydrothermal processes. *Science* 356:155-159.

Wiederschein, F., Vöhringer-Martinez, E., Beinsen, A., Postberg, F., Schmidt, J., Srama, R., Stolz, F., Grubmüller, H., and Abel, B. (2015) Charge separation and isolation in strong water droplet impacts. *Phys Chem Chem Phys* 17:6858-6864.

Wu, Y.C., Koch, W.F., Berezansky, P.A., and Holland, L.A. (1992) The Dissociation Constant of Amino Acids by the Conductimetric Method: I. pK<sub>1</sub> of MOPSO-HCl at 25°C. *J Solution Chem* 21:597-605.

Zsolnay, A. (1977) Inventory of nonvolatile fatty acids and hydrocarbons in the oceans. *Marine Chem* 5:465-475.

## Figure captions

**FIG. 1.** Formation of ice grains from heterogeneous nucleation (not to scale; from Postberg et al. 2018a with permission from Nature). (a) Ascending gas bubbles and thermal convection in the ocean transport organic material into water-filled cracks in the south polar ice crust. (b) Organics ultimately concentrate in a thin organic film/layer on top of the water table, located inside ice vents. When gas bubbles burst, they form aerosols made of organic material that later serve as condensation cores for the production of an icy crust from water vapor, thereby forming so-called HMOC-type (HMOC = High Mass Organic Cations) ice particles containing organic hydrophobic macromolecules. Another effect of the bubble bursting is that larger, pure saltwater droplets form, which freeze and are later detected as salt-rich so-called Type 3 ice particles in the plume and Saturn's E ring. The figure implies the parallel formation of both organic and saltwater spray, but their formation could actually be separated in space (e.g., at different tiger stripes cracks) or time (Postberg et al. 2018b).

**FIG. 2.** Laboratory analogue setup (the LILBID-TOF-MS apparatus) for simulating hypervelocity impacts of ice grains onto impact ionization mass spectrometers in space. The schematic (inset) shows the instrument configuration

underlying the principle of delayed extraction (taken from Klenner et al., 2019; adapted from Postberg et al., 2018a). The oil diffusion pump shown has recently been replaced by a turbo pump.

**FIG. 3.** Section of a baseline corrected cation mass spectrum of 100 ppmw His in 0.1 M NaCl (y-axis in logarithmic scale). The characteristic amino acid peaks are sodiated and detectable at His + 45 u (m/z 200) and His + 67 u (m/z 222). In addition to the amino acid peaks, the spectrum is dominated by salt peaks (unlabeled) from the matrix solution, with amplitudes often much higher than those of the amino acid (see text for further explanation).

**FIG. 4.** A section of a cation mass spectrum (216 - 221 u) of  $57 \times 10^{-5}$  M (100 ppmw) arginine in 0.1 M NaCl (y-axis in logarithmic scale). Although the salt cluster species  $[(\text{NaCl})_2(\text{NaOH})_2\text{Na}]^+$  at m/z 219 interferes with the sodiated  $[(\text{ArgNa})\text{Na}]^+$  (labeled blue), both species are identifiable. An extended mass range version of this spectrum is shown in Figure S1.

**FIG. 5.** Section (115 - 215 u) of a baseline corrected laboratory cation mass spectrum (y-axis in logarithmic scale) of the seven most abundant amino acids Gly,

Ala, ABA, Ser, Val, Asp, and Glu at abiotic concentration ratios in a salty Enceladus-like solution (Solution ii) containing background compounds (carboxylic acids). Only Ser is undetectable at its inferred abiotic concentration of  $2.9 \times 10^{-5}$  M. Concentrations can be found in Table S1, together with the calculation of the concentrations in Supplementary Material 1. The characteristic amino acid peaks are labeled in blue. In addition to the amino acid peaks, there are NaCl-water and  $\text{Na}_2\text{CO}_3$ -water peaks (unlabeled) from the matrix solution, with amplitudes often much higher than the amino acid peaks (see text for further explanation). No mass lines from the added carboxylic acids are observable.

**FIG. 6.** Top: Baseline corrected anion mass spectrum (y-axis in logarithmic scale) of fatty acids at abiotic concentration ratios in a water-acetonitrile matrix (50:50 vol) (adapted from Klenner et al., 2020). The characteristic fatty acid peaks are labeled red and green for even and odd carbon number fatty acids, respectively. Deprotonated molecular peaks are equally intense, in agreement with the fatty acids' equal concentrations of  $5.5 \times 10^{-6}$  M. Bottom: Baseline corrected anion mass spectrum (y-axis in logarithmic scale) of fatty acids at biotic concentration ratios in a water-acetonitrile matrix (50:50 vol; Solution type iii). Deprotonated molecular peak amplitudes reflect the concentration differences between odd and even carbon number fatty acids. Concentrations are  $5.5 \times 10^{-6}$  M for the odd carbon number fatty

acids C<sub>13</sub>, C<sub>15</sub>, C<sub>17</sub>, C<sub>19</sub>, 55 x 10<sup>-6</sup> M for the even carbon number fatty acids C<sub>12</sub>, C<sub>14</sub>, C<sub>20</sub> and 275 x 10<sup>-6</sup> M for C<sub>16</sub> and C<sub>18</sub>. Concentrations in ppmw can be found in Table S2. Fatty acid dimers (sodiated) from the most abundant compounds are observed at m/z > 450. The total carbon numbers of the dimers are labeled in purple as D<sub>28</sub>, D<sub>30</sub>, D<sub>32</sub>, D<sub>34</sub> and D<sub>36</sub>.

**FIG. 7.** Section of a baseline corrected laboratory mass spectrum (120 – 190 u) recorded in the cation mode of the mass spectrometer (y-axis in logarithmic scale). The measured solution contains amino acids at relative abundances chosen to be representative for biotic processes as well as carboxylic acids as background components (Solution type iv). The concentrations can be found in Table S3. The amino acids (labeled blue) are clearly identifiable. Peaks from the background carboxylic acids are labeled orange. Unlabeled peaks of the background matrix are from water clusters ( $[(\text{H}_2\text{O})_n\text{H}_3\text{O}]^+$ ), Na-water clusters ( $[(\text{H}_2\text{O})_n\text{Na}]^+$ ) or water clusters of the organics ( $[(\text{H}_2\text{O})_n\text{organic}]^+$ ).

**FIG. 8.** Two sections of a baseline corrected laboratory mass spectrum (70 – 140 u on the top panel and 160 – 350 u on the bottom panel) recorded in the anion mode of the mass spectrometer (y-axis in logarithmic scale). The solution contains amino acids and fatty acids at relative abundance ratios representative for biotic processes

and carboxylic acids as background components (Solution type iv). The concentrations can be found in Table S3. A water-acetonitrile (50:50 vol) matrix was used as the fatty acids are poorly water soluble. Amino acids (labeled blue) and fatty acids (labeled red and green) are clearly identifiable. Unspecified but fatty acid samples related peaks at  $m/z$  172 and  $m/z$  186 are observable as in Solution type iii. Peaks from the background carboxylic acids are labeled orange. Unlabeled peaks of the background matrix are from water clusters ( $[(H_2O)_nOH]^-$ ), Cl-water clusters ( $[(H_2O)_nCl]^-$ ) or water clusters of the organics ( $[(H_2O)_norganic]^-$ ).

**Table 1.** Detection limits for the LILBID results and molecular weights of amino acids in a salty 0.1 M NaCl solution. Note, that detection limits for space instruments will likely be lower than these values (see main text).

Amino acid ( <i>Three letter code</i> )	Molecular weight [u]	Detected ion	Detection limit [ $\mu\text{mol/L}$ ]	Detection limit [ppmw]
Aspartic acid ( <i>Asp</i> )	133	Asp + 45 u	15	2
		Asp + 67 u	4	0.5
Glutamic acid ( <i>Glu</i> )	147	Glu + 45 u	34	5
		Glu + 67 u	3	0.5
Histidine ( <i>His</i> )	155	His + 45 u	13	2
		His + 67 u	161	25
Arginine ( <i>Arg</i> )	174	Arg + 45 u	56	10
		Arg + 67 u	5740	1000
Citrulline ( <i>Cit</i> )	175	Cit + 45 u	117	20
		Cit + 67 u	286	50
Glycine ( <i>Gly</i> )	75	Gly + 45 u	270	20
Serine ( <i>Ser</i> )	105	Ser + 45 u	19	2
Threonine ( <i>Thr</i> )	119	Thr + 45 u	83	10
Ornithine ( <i>Orn</i> )	132	Orn + 45 u*	78	10

Tyrosine ( <i>Tyr</i> )	181	Tyr + 45 u	55	10
		Tyr + 67 u	11	2

\*We note that *Orn* produces an AA + 67 u peak with an amplitude lower than AA + 45 although the detection limit was not determined.

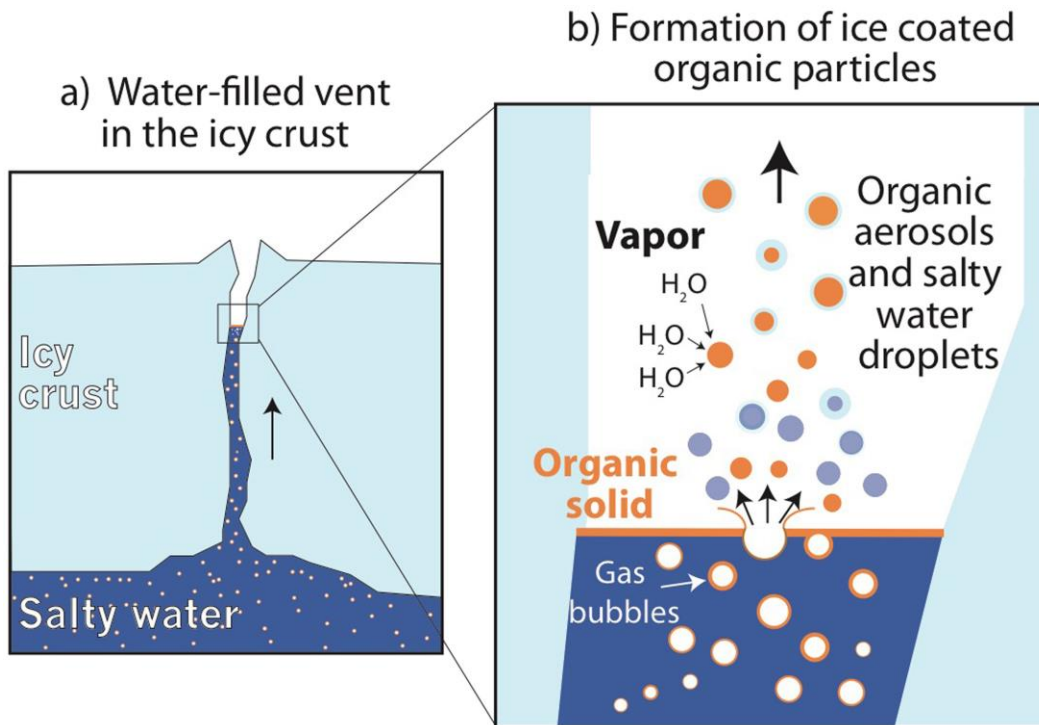


**FIG. 1.** Formation of ice grains from heterogeneous nucleation (not to scale; from Postberg et al. 2018a with permission from Nature). (a) Ascending gas bubbles and thermal convection in the ocean transport organic material into water-filled cracks in the south polar ice crust. (b) Organics ultimately concentrate in a thin organic film/layer on top of the water table, located inside ice vents. When gas bubbles burst, they form aerosols made of organic material that later serve as condensation cores for the production of an icy crust from water vapor, thereby forming so-called HMOC-type (HMOC = High Mass Organic Cations) ice particles containing organic hydrophobic macromolecules. Another effect of the bubble bursting is that larger, pure saltwater droplets form, which freeze and are later detected as salt-rich

so-called Type 3 ice particles in the plume and Saturn's E ring. The figure implies the parallel formation of both organic and saltwater spray, but their formation could actually be separated in space (e.g., at different tiger stripes cracks) or time (Postberg et al. 2018b).

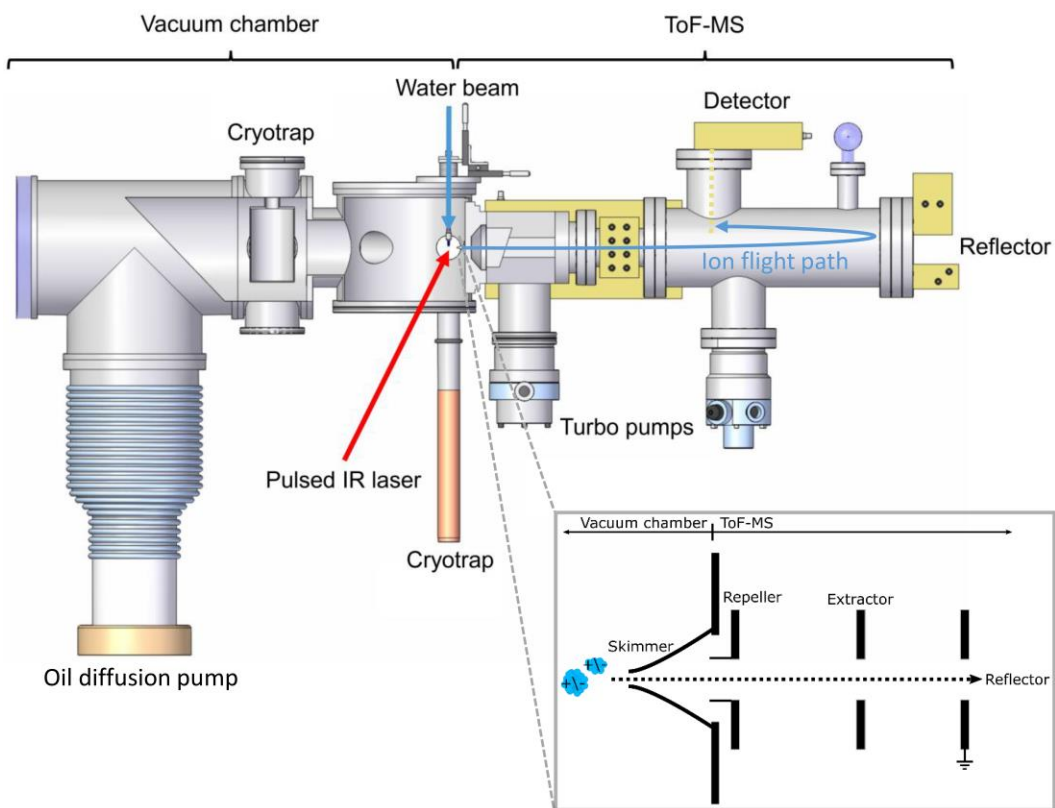


**FIG. 2.** Laboratory analogue setup (the LILBID-TOF-MS apparatus) for simulating hypervelocity impacts of ice grains onto impact ionization mass spectrometers in space. The schematic (inset) shows the instrument configuration underlying the principle of delayed extraction (taken from Klenner et al., 2019;

adapted from Postberg et al., 2018a). The oil diffusion pump shown has recently been replaced by a turbo pump.

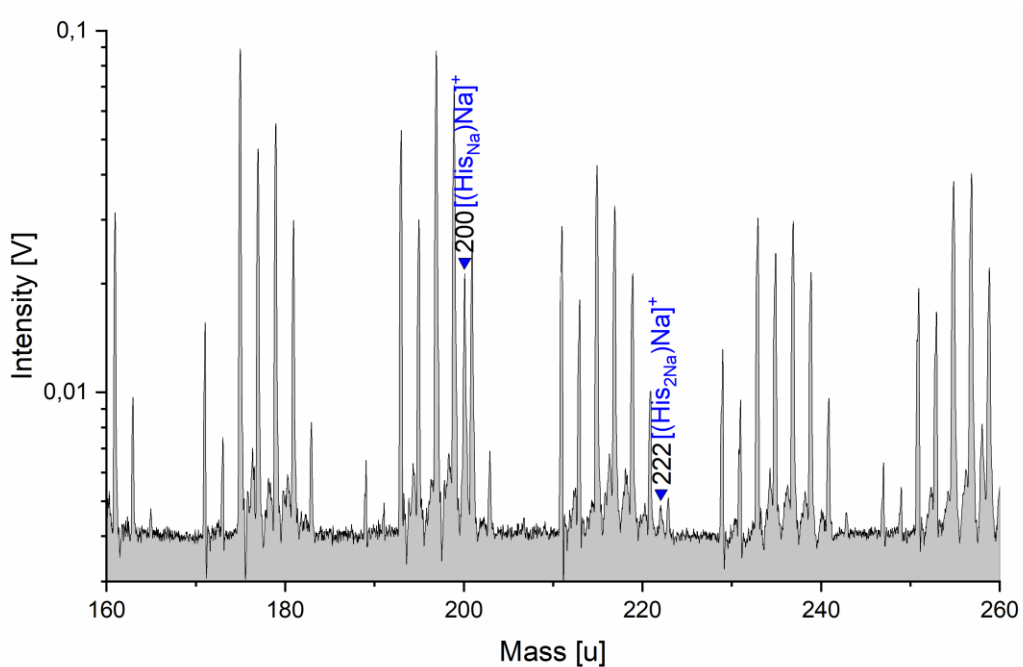


**FIG. 3.** Section of a baseline corrected cation mass spectrum of 100 ppmw His in 0.1 M NaCl (y-axis in logarithmic scale). The characteristic amino acid peaks are sodiated and detectable at His + 45 u (m/z 200) and His + 67 u (m/z 222). In addition to the amino acid peaks, the spectrum is dominated by salt peaks (unlabeled) from the matrix solution, with amplitudes often much higher than those of the amino acid (see text for further explanation).

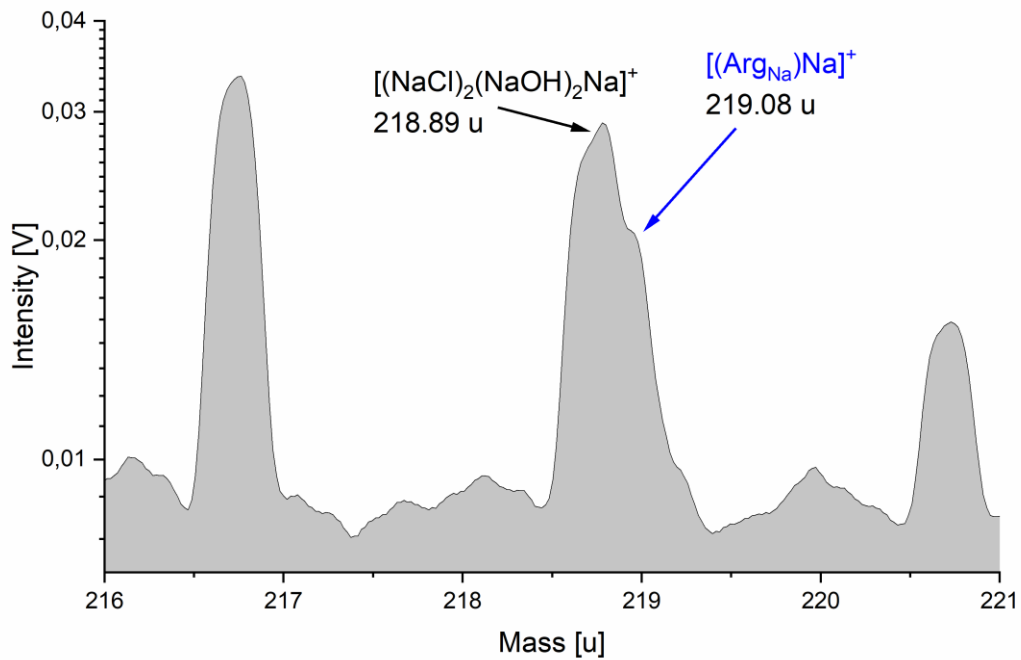


**FIG. 4.** A section of a cation mass spectrum (216 - 221 u) of  $57 \times 10^{-5}$  M (100 ppmw) arginine in 0.1 M NaCl (y-axis in logarithmic scale). Although the salt cluster species  $[(\text{NaCl})_2(\text{NaOH})_2\text{Na}]^+$  at  $m/z$  219 interferes with the sodiated  $[(\text{Arg}_{\text{Na}})\text{Na}]^+$  (labeled blue), both species are identifiable. An extended mass range version of this spectrum is shown in Figure S1.

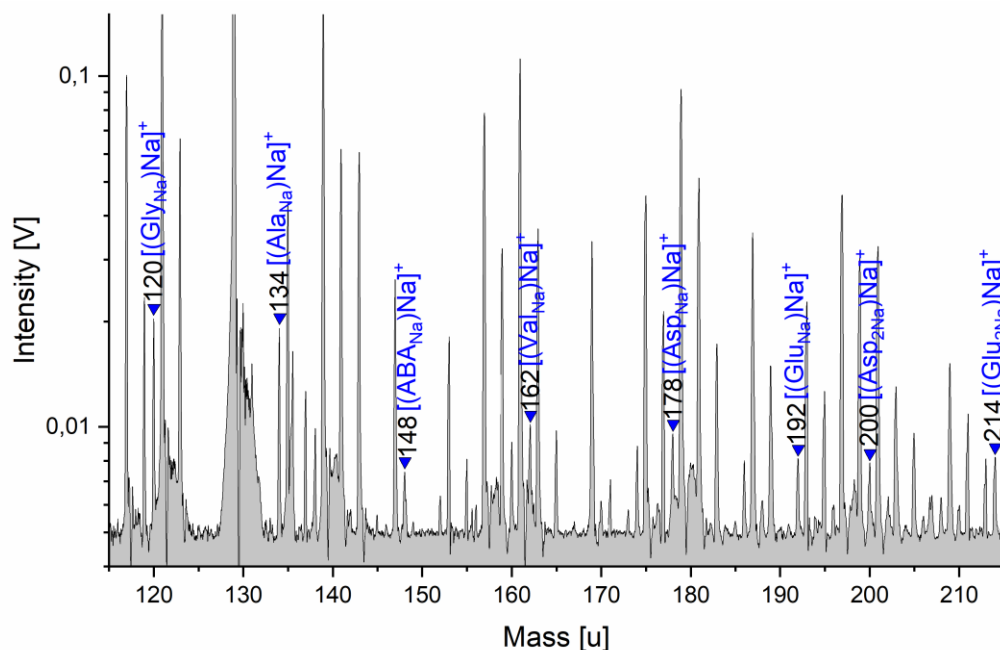


**FIG. 5.** Section (115 - 215 u) of a baseline corrected laboratory cation mass spectrum (y-axis in logarithmic scale) of the seven most abundant amino acids Gly, Ala, ABA, Ser, Val, Asp, and Glu at abiotic concentration ratios in a salty Enceladus-like solution (Solution ii) containing background compounds (carboxylic acids). Only Ser is undetectable at its inferred abiotic concentration of  $2.9 \times 10^{-5}$  M. Concentrations can be found in Table S1, together with the calculation of the concentrations in Supplementary Material 1. The characteristic amino acid peaks are labeled in blue. In addition to the amino acid peaks, there are NaCl-water and  $\text{Na}_2\text{CO}_3$ -water peaks (unlabeled) from the matrix solution, with amplitudes often much higher than the amino acid peaks (see text for further explanation). No mass lines from the added carboxylic acids are observable.

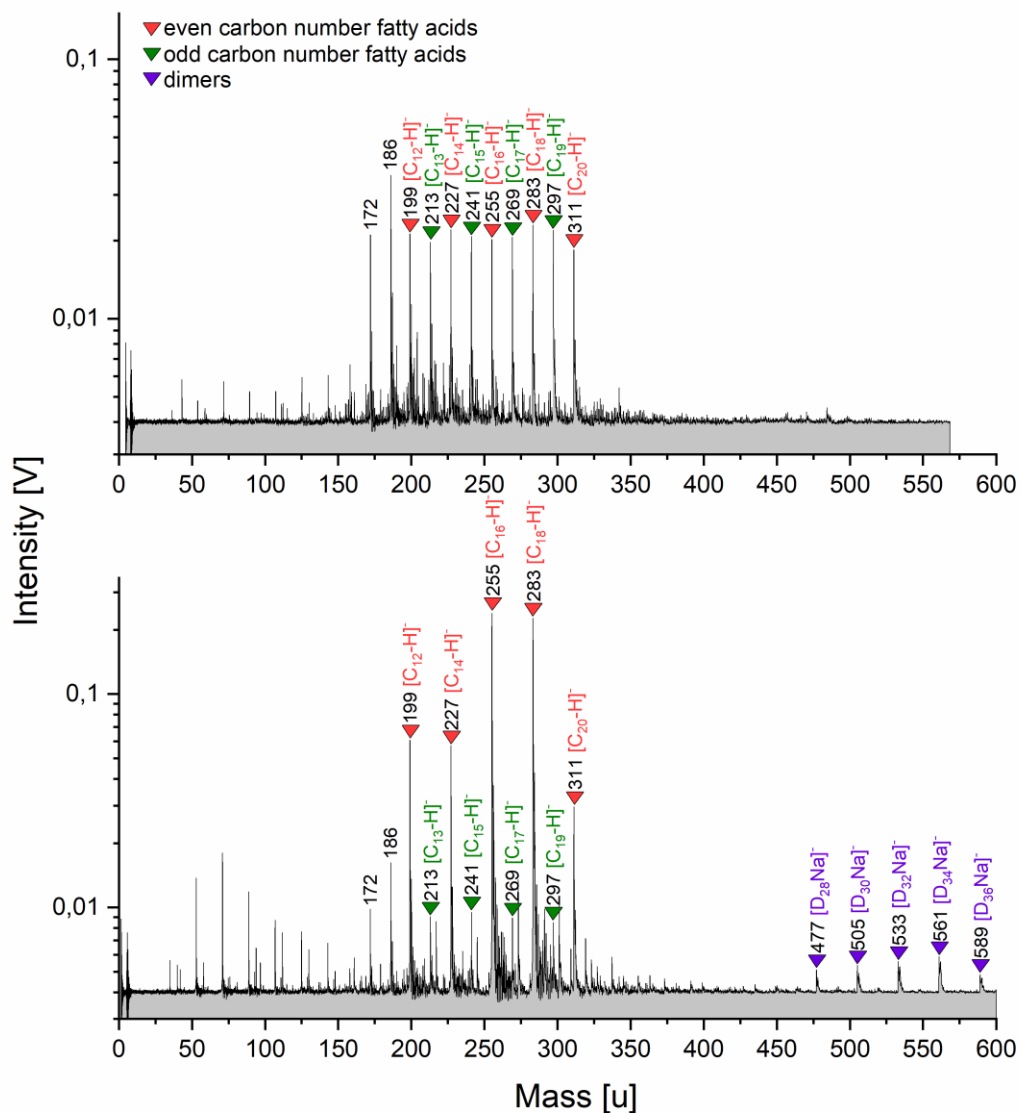


**FIG. 6.** Top: Baseline corrected anion mass spectrum (y-axis in logarithmic scale) of fatty acids at abiotic concentration ratios in a water-acetonitrile matrix (50:50 vol) (adapted from Klenner et al., 2020). The characteristic fatty acid peaks are

labeled red and green for even and odd carbon number fatty acids, respectively. Deprotonated molecular peaks are equally intense, in agreement with the fatty acids' equal concentrations of  $5.5 \times 10^{-6}$  M. Bottom: Baseline corrected anion mass spectrum (y-axis in logarithmic scale) of fatty acids at biotic concentration ratios in a water-acetonitrile matrix (50:50 vol; Solution type iii). Deprotonated molecular peak amplitudes reflect the concentration differences between odd and even carbon number fatty acids. Concentrations are  $5.5 \times 10^{-6}$  M for the odd carbon number fatty acids C<sub>13</sub>, C<sub>15</sub>, C<sub>17</sub>, C<sub>19</sub>,  $55 \times 10^{-6}$  M for the even carbon number fatty acids C<sub>12</sub>, C<sub>14</sub>, C<sub>20</sub> and  $275 \times 10^{-6}$  M for C<sub>16</sub> and C<sub>18</sub>. Concentrations in ppmw can be found in Table S2. Fatty acid dimers (sodiated) from the most abundant compounds are observed at  $m/z > 450$ . The total carbon numbers of the dimers are labeled in purple as D<sub>28</sub>, D<sub>30</sub>, D<sub>32</sub>, D<sub>34</sub> and D<sub>36</sub>.

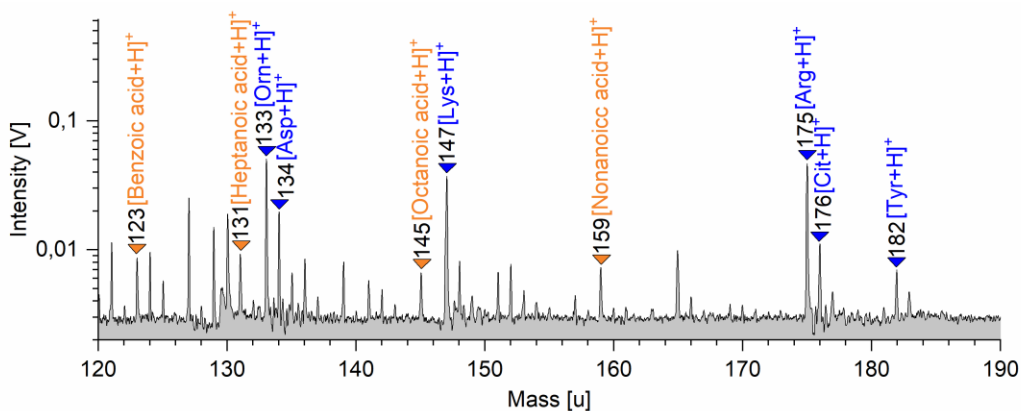


**FIG. 7.** Section of a baseline corrected laboratory mass spectrum (120 – 190 u) recorded in the cation mode of the mass spectrometer (y-axis in logarithmic scale). The measured solution contains amino acids at relative abundances chosen to be representative for biotic processes as well as carboxylic acids as background components (Solution type iv). The concentrations can be found in Table S3. The amino acids (labeled blue) are clearly identifiable. Peaks from the background carboxylic acids are labeled orange. Unlabeled peaks of the background matrix are from water clusters ( $[(\text{H}_2\text{O})_n\text{H}_3\text{O}]^+$ ), Na-water clusters ( $[(\text{H}_2\text{O})_n\text{Na}]^+$ ) or water clusters of the organics ( $[(\text{H}_2\text{O})_n\text{organic}]^+$ ).

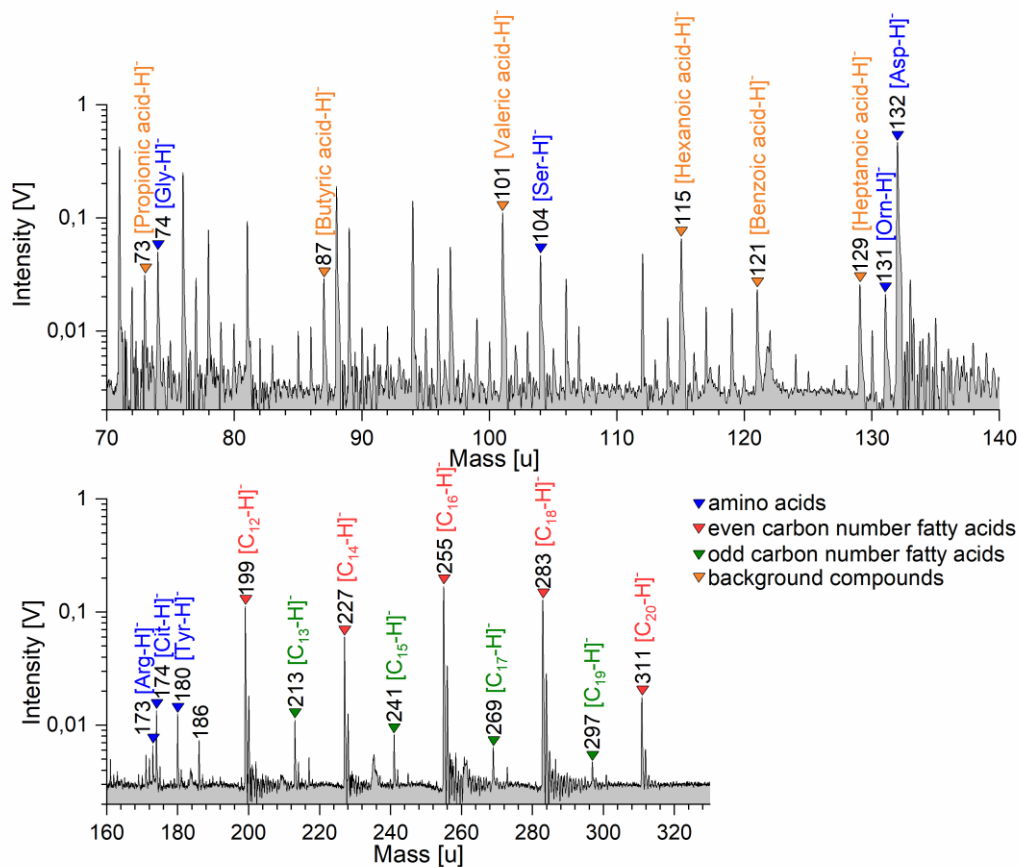


**FIG. 8.** Two sections of a baseline corrected laboratory mass spectrum (70 – 140 u on the top panel and 160 – 350 u on the bottom panel) recorded in the anion mode of the mass spectrometer (y-axis in logarithmic scale). The solution contains amino acids and fatty acids at relative abundance ratios representative for biotic processes and carboxylic acids as background components (Solution type iv). The concentrations can be found in Table S3. A water-acetonitrile (50:50 vol) matrix was used as the fatty acids are poorly water soluble. Amino acids (labeled blue) and fatty acids (labeled red and green) are clearly identifiable. Unspecified but fatty

acid samples related peaks at  $m/z$  172 and  $m/z$  186 are observable as in Solution type iii. Peaks from the background carboxylic acids are labeled orange. Unlabeled peaks of the background matrix are from water clusters ( $[(\text{H}_2\text{O})_n\text{OH}]^-$ ), Cl-water clusters ( $[(\text{H}_2\text{O})_n\text{Cl}]^-$ ) or water clusters of the organics ( $[(\text{H}_2\text{O})_n\text{organic}]^-$ ).

**Supplementary Material 1: Calculation of the amino acid concentrations in Table S1 (Solution type ii) using glutamic acid (Glu) as an example.**

Published Glu concentrations in a selection of CR chondrites (Glavin et al., 2011; Pizzarello et al. 2012) are 1.6  $\mu\text{mol/kg}$ , 8.2  $\mu\text{mol/kg}$ , 16.4  $\mu\text{mol/kg}$ , 9.4  $\mu\text{mol/kg}$  and 16.7  $\mu\text{mol/kg}$ , means 10.46  $\mu\text{mol/kg}$  on average. 10.46  $\mu\text{mol/kg}$  equates to 1.54 mg/kg.

Using two different estimates of the total mass of Enceladus: I.  $8.38 \times 10^{19}$  kg and II.  $6.3 \times 10^{19}$  kg (Waite et al., 2017, supplement therein) gives the total amino acid mass on Enceladus:

- I.  $1.54 \text{ mg/kg} \times 8.38 \times 10^{19} \text{ kg} = 1.29 \times 10^{14} \text{ kg}$
- II.  $1.54 \text{ mg/kg} \times 6.3 \times 10^{19} \text{ kg} = 9.69 \times 10^{13} \text{ kg}$

With two different estimates of the ocean mass of the Enceladean ocean: I.  $3.2 \times 10^{19}$  kg and II.  $1 \times 10^{19}$  kg (Waite et al., 2017, supplement therein) the concentration of Glu in the Enceladean ocean is calculated as follows (assuming water-rock interaction):

- I.  $1.29 \times 10^{14} \text{ kg} / 3.2 \times 10^{19} \text{ kg} = 4.03 \text{ ppmw}$
- II.  $9.69 \times 10^{13} \text{ kg} / 1 \times 10^{19} \text{ kg} = 9.69 \text{ ppmw}$

4.03 ppmw and 9.69 ppmw means 6.86 ppmw on average.

A conservative concentration towards the lower end of this range, 5 ppmw, was chosen for the abiotic mix.

**Table S1.** Concentrations in the abiotic amino acid mix (Solution type ii) used for the mass spectrum in Figure 5. For calculations of the concentrations see section Biosignature solutions in the main text and Supplementary Material 1. Amino acids and carboxylic acids are separately listed in order of decreasing concentration in  $\mu\text{mol/L}$ .

Amino acid	Molecular weight [u]	Concentration [ $\mu\text{mol/L}$ ]	Concentration [ppmw]
Gly	75	2000	150
Ala	89	1685	150
Val	117	641	75
ABA	103	388	40
Glu	147	34	5
Ser	105	29	3
Asp	133	15	2
Carboxylic acid	Molecular weight [u]	Concentration [ $\mu\text{mol/L}$ ]	Concentration [ppmw]

Valeric acid	102	588	60
Methylbutyric acid	102	588	60
Hexanoic acid	116	259	30
Acetic acid	60	250	15
Heptanoic acid	130	231	30
Butyric acid	88	227	20
Octanoic acid	144	208	30
Nonanoic acid	158	190	30
Methylpentanoic acid	116	172	20
Ethylhexanoic acid	144	139	20
Benzoic acid	122	82	10
Formic acid	46	43	2
Ethylbutyric acid	116	43	5
Decanoic acid	172	29	5
Matrix component	Molecular weight	Concentration	
	[u]	[M]	
NaCl	58	0.1	
Na <sub>2</sub> CO <sub>3</sub>	106	0.015	
NaHCO <sub>3</sub>	84	0.015	
NH <sub>3</sub>	17	0.01	

**Table S2.** Fatty acid concentrations in biotic concentration ratios used for the mass spectrum in Figure 6 (lower panel). The fatty acids are listed in order of decreasing concentration in  $\mu\text{mol/L}$ .

Fatty acid	Molecular weight [u]	Concentration [ $\mu\text{mol/L}$ ]	Concentration [ppmw]
C16	256	275	70
C18	284	275	78
C12	200	55	11
C14	228	55	13
C20	312	55	17
C13	214	5.5	1.2
C15	242	5.5	1.3
C17	270	5.5	1.5
C19	298	5.5	1.6

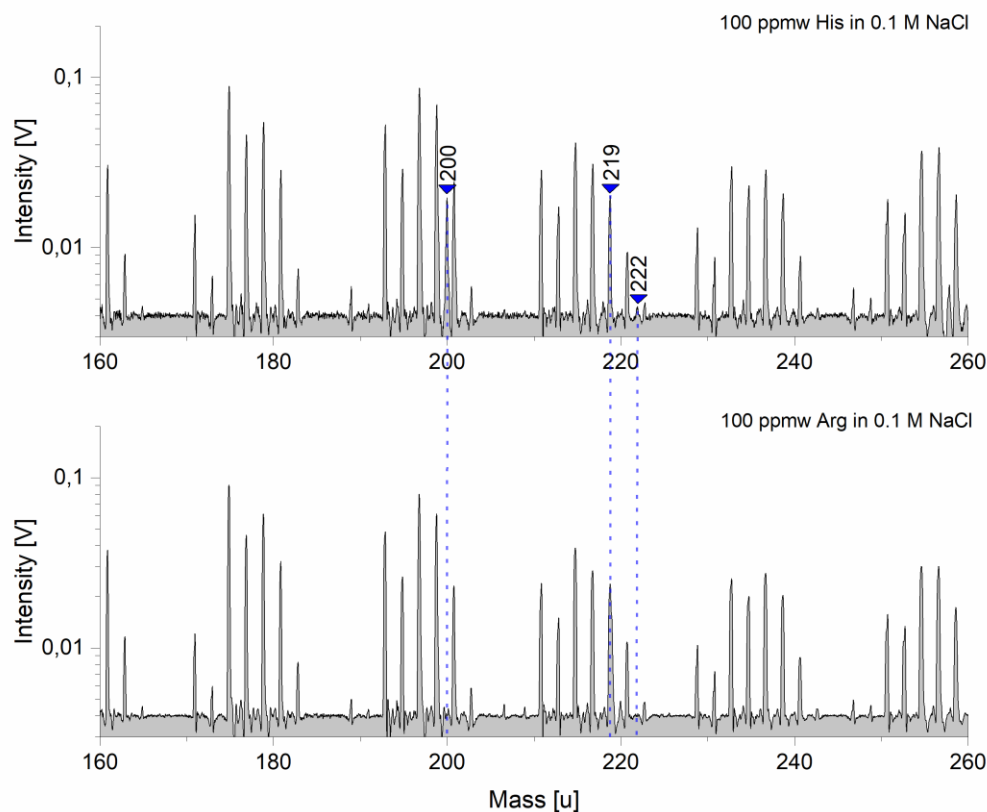
**Table S3.** Concentrations of the biotic organic mixes (Solution type iv) used for the mass spectra in Figure 7 and 8. The fatty acids were only used for the mass

spectra in Figure 8. Amino acids, fatty acids and carboxylic acids are separately listed in order of decreasing concentration in  $\mu\text{mol/L}$ .

Amino acid	Molecular weight [u]	Concentration [ $\mu\text{mol/L}$ ]	Concentration [ppmw]
Ser	105	29	3
Gly	75	27	2
Tyr	181	11	2
Cit	175	11	2
Asp	133	8	1
Orn	132	8	1
Arg	174	3	0.5
Lys	146	3	0.5
Fatty acid	Molecular weight [u]	Concentration [ $\mu\text{mol/L}$ ]	Concentration [ppmw]
C <sub>16</sub>	256	20	5
C <sub>18</sub>	284	18	5
C <sub>12</sub>	200	5	1
C <sub>14</sub>	228	4	1
C <sub>20</sub>	312	3	1
C <sub>13</sub>	214	0.5	0.1

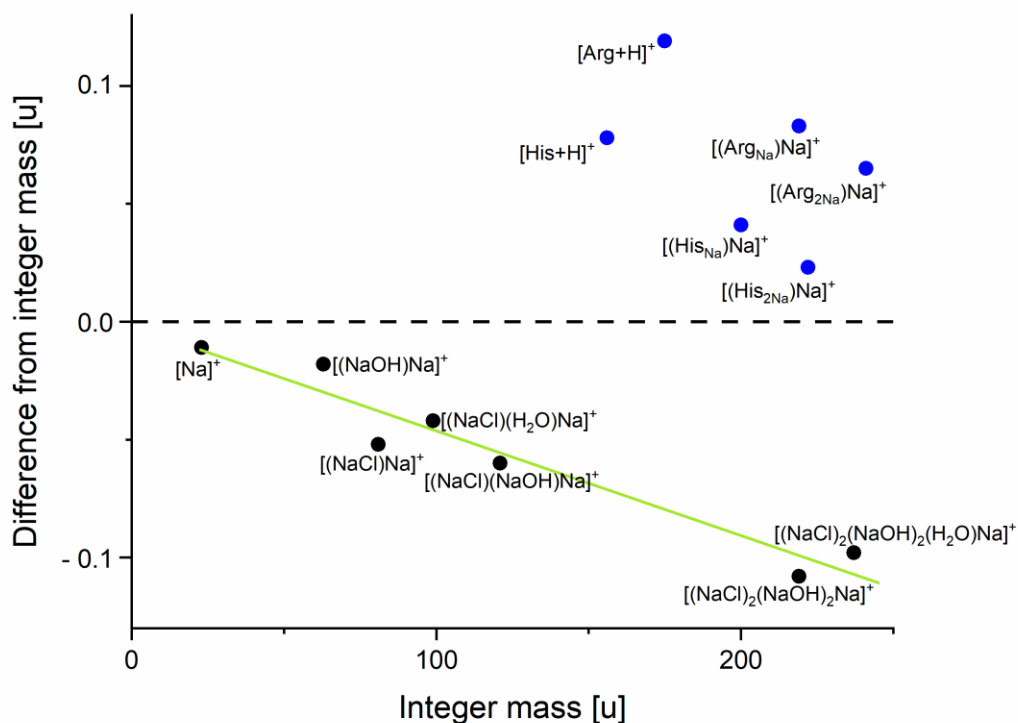
C <sub>15</sub>	242	0.4	0.1
C <sub>17</sub>	270	0.4	0.1
C <sub>19</sub>	298	0.3	0.1
Background compound	Molecular weight [u]	Concentration [μmol/L]	Concentration [ppmw]
Methylbutyric acid	102	539	55
Valeric acid	102	392	40
Hexanoic acid	116	259	30
Acetic acid	60	250	15
Butyric acid	88	227	20
Methylpentanoic acid	116	216	25
Octanoic acid	144	208	30
Nonanoic acid	158	158	25
Heptanoic acid	130	154	20
Ethylhexanoic acid	144	139	20
Benzoic acid	122	82	10
Ethylbutyric acid	116	43	5
Formic acid	46	43	2
Decanoic acid	172	29	5
Propionic acid	74	27	2

NaCl	58	9	0.5
------	----	---	-----



**Supplementary Material Figure S1:** Sections (160 – 260 u) of baseline corrected cation mass spectra (y-axis in logarithmic scale) of 100 ppmw His in 0.1 M NaCl (top) and 100 ppmw Arg in 0.1 M NaCl (bottom). The two solutions differ only in the amino acid (His or Arg) used. Both spectra show identical peaks from the matrix solution with nearly identical amplitudes. His is clearly identifiable as disodiated cation  $[(\text{HisNa})\text{Na}]^+$  at  $m/z$  200 and as trisodiated cation  $[(\text{His}_2\text{Na})\text{Na}]^+$  at  $m/z$  222

(top). The disodiated arginine cation  $[(\text{Arg}_{\text{Na}})\text{Na}]^+$  interferes with the salt species  $[(\text{NaCl})_2(\text{NaOH})_2\text{Na}]^+$  from the matrix solution at  $m/z$  219 (bottom). This interference can be resolved with the available mass resolution of 600-800  $m/\Delta m$  because of a significant peak asymmetry (Figure 4).



**Supplementary Material Figure S2:** Masses on the integer level vs. exact differences from integer masses of the most common isotopes of typical salt species as seen in LILBID spectra of salt rich solutions (black dots) and unsodiated as well as sodiated species of two amino acids (His and Arg; blue dots). Salt species from

a salty background solution have a negative offset with respect to the integer mass. The masses of these salt and (unsodiated and sodiated) amino acid species near the same integer mass typically differ by about 0.15 – 0.2 u. The green trend line (applied to the salt species) highlights that the salt species' negative mass differences increase with mass.